

**The study of stability of compression-loaded
multispan composite panel upon failure of elements
binding it to panel supports**

Prepared by:

G.N.Zamula

K.M.Ierusalimsky

V.P.Fomin

V.I.Grishin

G.S.Kalmykova

ABSTRACT

The present document is a final technical report under the NCC-1-233 research program (dated September 15, 1998; see Appendix 5) carried out within co-operation between United States' NASA Langley RC and Russia's Goskomoboronprom in aeronautics, and continues similar programs, NCCW-73, NCC-1-233 and NCCW 1-233 accomplished in 1996, 1997, and 1998, respectively.

The report provides results of "The study of stability of compression-loaded multispan composite panels upon failure of elements binding it to panel supports"; these comply with requirements established at TsAGI on 24 March 1998 and at NASA on 15 September 1998.

Table of Contents

INTRODUCTION.....	4
Part 1. The method for studying stability of compression-loaded stiffened multispan composite panel after failure of elements binding it to transverse and longitudinal supports	5
1.1. Solution to the problem of postbuckling behavior of unsupported part in compression-loaded multispan panel upon failure of support links.....	5
1.2. Dependence of ultimate load on panel parameters and link fracture energy available: A parametric study.....	15
Part 2. Fracture energy and strength of links between the multispan panel and supports: Critical values for ensuring traditional buckling with nodal lines being on the supports.....	19
2.1. The method to evaluate link fracture energy for bolted and riveted joints; relation to load-displacement diagram and bolt/rivet fracture load.....	20
2.2. Finite element analysis of link fracture energy for bolted joints	21
2.3. Establishing parameters necessary to ensure a specified panel-to-support link strength.....	30
CONCLUSION.....	34
LITERATURE.....	35
APPENDIX.....	36

INTRODUCTION

The previous studies in [1, 2] paid major attention, firstly, to postbuckling behavior of composite panels and, secondly, to the problem of evaluating strength and buckling of a built-up structure with consideration of postbuckling deformation of some components. These studies relied on the assumption that the thin-walled elements are attached to supports by links which do not fail until the structure becomes destroyed.

However, the links may turn out to have inadequate strength, and the structure can fail due to fracture of the links between the panel and supports. This outcome is evidenced by static strength testing of a number of real structures. Figure 0.1 demonstrates airplane wing fracture; one can see that the upper, compression-loaded panel has failed because of fracture of links between the panel and ribs when the load was much less than the critical value obtained under the assumption that the buckling nodal lines rest on the ribs.

The present research suggests the approach which enables predicting the panel failure load as a function of strength of particular links between the panel and supports.

Let us detail now the essence of the problem.

One knows that the major load for upper panels in a large-aspect-ratio wing is the longitudinal compression caused by general bending. Therefore, parameters of upper stiffened panels (including the rib spacing) are specified on the basis of critical stress resultants N_{cr}^* which are computed under the assumption that ribs are nodal lines for the buckled panel.

This approach is valid if strength of links between the continuous panel and rib/spar flanges is sufficient for the buckling mode above.

However, if not, the panel may buckle at a load N_{x0} less than N_{cr}^* , upon failure of links along one or more supports.

Thus, there appears the problem of predicting the necessary strength of links between a compression-loaded panel and the supports (i.e., ribs and spars) – such that the panel buckling nodal lines be on supports; this problem is rather challenging in case a high stress must be applied to a monolithic composite stiffened panel.

The problem is treated here by using the energy method proposed in [3] for analyzing behavior of a compression-loaded composite plate with delamination.

Note that analyzing the strength of links between the panel and intermediate supports is different from the usual problem of searching for the necessary stiffness of compliant support; the latter formulation proceeds from buckling shapes caused by mutual deformation of the supports and permanently attached panel.

Part 1. The method for studying stability of compression-loaded stiffened multispan composite panel after failure of elements binding it to transverse and longitudinal supports

1.1. Solution to the problem of postbuckling behavior of unsupported part in compression-loaded multispan panel upon failure of support links

Let us consider a rectangular flat orthotropic panel incorporated in a thin-walled wing torsion box (Fig. 1.1). The panel is attached to rib flanges, and its sides, to spar flanges. Panel parameters are

- L , the length,
- b , the width,
- a , the rib spacing;

clearly, $L = k_m a$ where k_m is the total number of panel bays. At the ends the panel is compressed with stress resultants N_{x_0} .

The subcritical (flat) state of the panel (the state I in Fig. 1.2) is characterized with the resultant N_{x_0} and the in-plane displacement Δ_x .

At a certain value of N_{x_0} the panel can buckle over a certain length $\ell = k a$ (where k is an integer), which process makes the panel be separated from $k - 1$ ribs – refer to state II in Fig. 1.2.

The other buckling mode is panel buckling over a certain length ℓ with separation from $k - 1$ ribs and two longitudinal supports (that is spars) – refer to state III in Fig. 1.2.

If the panel is connected to ribs and spars by rather strong links, then the major buckling shape is the usual sinusoidal surface whose nodal lines are on ribs and spars – see state III in Fig. 1.2; in this case the critical load N_{cr}^* is calculated by usual formulas.

Let us address now panel buckling with transition from state I to state II (Fig. 1.2).

Assume that the panel in its subcritical condition is compressed with the stress resultant N_{x_0} ; the panel ends have a mutual longitudinal displacement Δ_x . The panel energy U is equivalent to the triangle area $\frac{1}{2} N_{x_0} \Delta_x$, Fig. 1.3. Upon failure of rib links the panel buckles over a portion of length ℓ , and the load gets decreased to \overline{N}_{x_0} . With the state II implemented, the displacement Δ_x does not change. The total initial compression energy U transforms into

– compression energy \overline{U}_p and

– bending energy \overline{U}_b ,

and the panel has an out-of-plane displacement f . The difference of energy between states I and II,

$$R = U - (\overline{U}_p + \overline{U}_b) \quad (1.1)$$

is released when the links fail. Energy balance equation (1.1) is represented graphically in Fig. 1.3; here, R is the work for destroying the links between the panel and ribs during buckling over the length $\ell = ka$.

Thus, energy balance equation (1.1) and the condition $\Delta_x = \text{const}$ for the transition from state I to state II make it possible to determine N_{x0} and the final out-of-plane displacement f . The buckling surface length $\ell = ka$ is evaluated by minimizing N_{x0} with respect to k .

We should relate the compression energy U and the mutual displacement Δ_x to other variables in the problem.

Strains and stress resultants in the midsurface of the orthotropic panel are interrelated as follows:

$$\varepsilon_x = A_{11} N_x + A_{12} N_y, \quad \varepsilon_y = A_{12} N_x + A_{22} N_y, \quad \gamma = A_{33} N_{xy}, \quad (1.2)$$

where A_{11} , A_{22} , A_{33} and A_{12} are cocos of compliance of the panel in its plane. The mutual end displacement may be expressed as,

$$\Delta_x = L A_{11} N_{x0}. \quad (1.3)$$

Compression potential energy is,

$$U = Lb \frac{A_{11}}{2} N_{x0}^2. \quad (1.4)$$

To compute the bending energy component \overline{U}_b and the compression energy component \overline{U}_p , we consider the panel buckled over the length ℓ . Assume that the plain (not buckled) parts of the panel clamp the transverse edges $\{x = 0\}$ and $\{x = \ell\}$ of the separated part.

In case the panel is torn off the ribs only, the out-of-plane displacement is expressed as,

$$w = f \sin^2 \frac{\pi x}{\ell} \sin \frac{\pi y}{b}. \quad (1.5)$$

The midsurface stress resultants are determined by solving the deformation compatibility equation from [4]:

$$\frac{\partial^2 \varepsilon_x}{\partial y^2} + \frac{\partial^2 \varepsilon_y}{\partial x^2} - \frac{\partial^2 \gamma}{\partial x \partial y} = \frac{1}{2} \mathcal{L}(w, w), \quad (1.6)$$

where we use the nonlinear operator

$$\frac{1}{2} \mathcal{L}(w, w) = \left(\frac{\partial^2 w}{\partial x \partial y} \right)^2 - \frac{\partial^2 w}{\partial x^2} \frac{\partial^2 w}{\partial y^2},$$

and midsurface strains are

$$\varepsilon_x = \frac{\partial u}{\partial x} + \frac{1}{2} \left(\frac{\partial w}{\partial x} \right)^2, \quad \varepsilon_y = \frac{\partial v}{\partial y} + \frac{1}{2} \left(\frac{\partial w}{\partial y} \right)^2, \quad \gamma = \frac{\partial u}{\partial y} + \frac{\partial v}{\partial x} + \frac{\partial w}{\partial x} \frac{\partial w}{\partial y}. \quad (1.7)$$

Now, stress resultants N_x , N_y and N_{xy} are expressed in terms of the function Φ :

$$N_x = \frac{\partial^2 \Phi}{\partial y^2}, \quad N_y = \frac{\partial^2 \Phi}{\partial x^2}, \quad N_{xy} = -\frac{\partial^2 \Phi}{\partial x \partial y}, \quad (1.8)$$

and substituted (with ε_x , ε_y , and γ from (1.7) and w from (1.5)) into the formula (1.6) to obtain the following equation:

$$\mathcal{L}_1(\Phi) = \frac{1}{2} \mathcal{L}(w, w), \quad (1.9)$$

where

$$\mathcal{L}_1(\Phi) = A_{22} \frac{\partial^4 \Phi}{\partial x^4} + 2A_3 \frac{\partial^4 \Phi}{\partial x^2 \partial y^2} + A_{11} \frac{\partial^4 \Phi}{\partial y^4}, \quad (1.10)$$

$$A_3 = A_{12} + \frac{1}{2} A_{33}.$$

The relation (1.5) is to be substituted in the right-hand side of (1.6) to obtain

$$\frac{1}{2} \mathcal{L}(w, w) = \frac{f^2}{2} \frac{\pi^4}{\ell^4} \alpha^2 \left(\cos \frac{2\pi x}{\ell} - \cos \frac{4\pi x}{\ell} + \cos \frac{2\pi y}{b} - \cos \frac{2\pi x}{\ell} \cos \frac{2\pi y}{b} \right), \quad (1.11)$$

where

$$\alpha = \frac{\ell}{b}.$$

The general solution to (1.9) looks like this:

$$\Phi = \Phi_1 - N_{x0} \frac{y^2}{2}, \quad (1.12)$$

where

$$\Phi_1 = \frac{f^2}{32} \left[\alpha^2 \delta_2 \left(\cos \frac{2\pi x}{\ell} - \frac{1}{16} \cos \frac{4\pi x}{\ell} \right) + \frac{\delta_1}{\alpha^2} \cos \frac{2\pi y}{b} - a^2 \delta_3 \cos \frac{2\pi x}{\ell} \cos \frac{2\pi y}{b} \right],$$

$$\delta_1 = \frac{1}{A_{11}}, \quad \delta_2 = \frac{1}{A_{22}}, \quad \delta_3 = \frac{1}{A_{22} + 2A_3 \alpha^2 + A_{11} \alpha^4}.$$

Taking into account (1.12), the stress resultants N_x , N_y , and N_{xy} in (1.8) can be represented in terms of coordinates:

$$\left. \begin{aligned} N_x &= -\bar{N}_{x0} - t^2 \left(\delta_1 \cos \frac{2\pi y}{b} - \delta_3 \alpha^4 \cos \frac{2\pi x}{\ell} \cos \frac{2\pi y}{b} \right), \\ N_y &= -t^2 \alpha^2 \left[\delta_2 \left(\cos \frac{2\pi x}{\ell} - \frac{1}{4} \cos \frac{4\pi x}{\ell} \right) - \delta_3 \cos \frac{2\pi x}{\ell} \cos \frac{2\pi y}{b} \right], \\ N_{xy} &= t^2 \alpha^3 \delta_3 \sin \frac{2\pi x}{\ell} \sin \frac{2\pi y}{b}, \end{aligned} \right\} \quad (1.13)$$

where

$$t^2 = \frac{f^2}{8} \frac{\pi^2}{\ell^2}.$$

The equation of bending for the orthotropic panel in question may be written on the basis of [4]:

$$D_{11} \frac{\partial^4 w}{\partial x^4} + 2D_3 \frac{\partial^4 w}{\partial x^2 \partial y^2} + D_{22} \frac{\partial^4 w}{\partial y^4} - N_x \frac{\partial^2 w}{\partial x^2} - N_y \frac{\partial^2 w}{\partial y^2} - 2N_{xy} \frac{\partial^2 w}{\partial x \partial y} = 0, \quad (1.14)$$

where D_{11} , D_{22} , and D_3 are the panel bending stiffness parameters; these could be using [2] be related to stiffnesses of the orthotropic skin and stiffeners.

The dependence of panel out-of-plane displacement on the external load \bar{N}_{x0} is evaluated by solving Bubnov-Galerkin equation:

$$I = \int_0^{\ell} \int_0^b \bar{X} \sin^2 \frac{\pi x}{\ell} \sin \frac{\pi y}{b} dx dy = 0,$$

where \bar{X} is the left-hand side expression in (1.14). By allowing for (1.5) and (1.13), we derive,

$$\begin{aligned} I &= f \frac{\pi^2}{\ell^2} \int_0^{\ell} \int_0^b \left\{ \frac{\pi^2}{\ell^2} \left[-\left(8D_{11} + 2\alpha^2 D_3 \right) \cos \frac{2\pi x}{\ell} \sin \frac{\pi y}{b} + \alpha^4 D_{22} \sin^2 \frac{\pi x}{\ell} \sin \frac{\pi y}{b} \right] - \right. \\ &- \left[\bar{N}_{x0} + 2t^2 \left(\delta_1 - \delta_3 \alpha^4 \cos \frac{2\pi x}{\ell} \right) \cos \frac{2\pi y}{b} \right] \cos \frac{2\pi x}{\ell} \sin \frac{\pi y}{b} - t^2 \alpha^4 \left[\delta_2 \left(\cos \frac{2\pi x}{\ell} - \frac{1}{4} \cos \frac{4\pi x}{\ell} \right) - \right. \\ &- \left. \left. \delta_3 \cos \frac{2\pi x}{\ell} \cos \frac{2\pi y}{b} \right] \sin^2 \frac{\pi x}{\ell} \sin \frac{\pi y}{b} - 2t^2 \alpha^4 \delta_3 \sin^2 \frac{2\pi x}{\ell} \sin \frac{2\pi y}{b} \cos \frac{\pi y}{b} \right\} \sin^2 \frac{\pi x}{\ell} \sin \frac{\pi y}{b} dx dy = 0. \end{aligned}$$

By estimating the integrals and stipulating $f \neq 0$, the following relation appears:

$$4 \frac{\pi^2}{\ell^2} \left(D_{11} + \frac{1}{2} \alpha^2 D_3 + \frac{3}{16} \alpha^4 D_{22} \right) - \bar{N}_{x0} + \frac{t^2}{2} \left[\delta_1 + \alpha^4 \left(\frac{17}{16} \delta_2 + \frac{1}{2} \delta_3 \right) \right] = 0.$$

Hereinafter, the new symbols are utilized:

$$N_{cr}^{\Pi} = \frac{\pi^2 D_{11}}{a^2} \cdot k_{cr}^{\Pi}, \quad k_{cr}^{\Pi} = \frac{4}{k^2} \left(1 + \frac{1}{2} \alpha^2 \frac{D_3}{D_{11}} + \frac{3}{16} \alpha^4 \frac{D_{22}}{D_{11}} \right),$$

$$0 \leq \alpha = k \frac{a}{b} \leq \sqrt[4]{4 \frac{D_{11}}{D_{22}}},$$

$$\delta_4 = \frac{1}{2} \left(\delta_1 + \frac{17}{16} \alpha^4 \delta_2 + \frac{1}{2} \alpha^4 \delta_3 \right),$$

In these terms,

$$t^2 = \frac{1}{\delta_4} \left(\bar{N}_{x_0} - N_{cr}^{\Pi} \right). \quad (1.16)$$

The mutual in-plane displacement of the edges $\{x = 0\}$ and $\{x = L\}$ is,

$$\bar{\Delta}_x = - \int_0^L \frac{\partial u}{\partial x} dx.$$

Herein, the component from (1.7)

$$\frac{\partial u}{\partial x} = \varepsilon_x - \frac{1}{2} \left(\frac{\partial w}{\partial x} \right)^2,$$

should be substituted; and formulas (1.2), (1.5), and (1.13) have to be taken into account to produce

$$\bar{\Delta}_x = \frac{L}{\delta_1} \bar{N}_{x_0} + \int_0^L t^2 \left(\cos \frac{2\pi y}{b} + 4 \sin^2 \frac{2\pi x}{\ell} \sin^2 \frac{\pi y}{b} \right) dx,$$

or, substituting t^2 from (1.16):

$$\bar{\Delta}_x = \frac{L}{\delta_4} \left[\left(\bar{\delta}_4 + \bar{\ell} \right) \bar{N}_{x_0} - \bar{\ell} N_{cr}^{\Pi} \right], \quad (1.17)$$

where $\bar{\delta}_4 = \delta_4 / \delta_1$ and $\bar{\ell} = \ell / L$.

To determine external load \bar{N}_{x_0} applied to the buckled portion, we make use of the condition $\bar{\Delta}_x = \text{const}$ in case the panel comes from state I into state II. Allowing for (1.3) and (1.17), the result is,

$$\bar{N}_{x_0} = \frac{\bar{\delta}_4 N_{x_0} + \bar{\ell} N_{cr}^{\Pi}}{\bar{\delta}_4 + \bar{\ell}}, \quad (1.18)$$

Potential energy \bar{U} of the compression-bent panel is to be subdivided into the bending energy component \bar{U}_b and the midsurface deformation energy component \bar{U}_p :

$$\bar{U} = \bar{U}_b + \bar{U}_p. \quad (1.19)$$

The bending energy component may be written as

$$\bar{U}_b = \frac{1}{2} \int_0^\ell \int_0^b \left[D_{11} \left(\frac{\partial^2 w}{\partial x^2} \right)^2 + 2D_{12} \frac{\partial^2 w}{\partial x^2} \frac{\partial^2 w}{\partial y^2} + D_{22} \left(\frac{\partial^2 w}{\partial y^2} \right)^2 + 4D_{33} \left(\frac{\partial^2 w}{\partial x \partial y} \right)^2 \right] dx dy .$$

By substituting w from (1.5) into the above expression, we obtain

$$\bar{U}_b = 2 \frac{\pi^4}{\ell^4} f^2 \int_0^\ell \int_0^b \left[\left(D_{11} \cos^2 \frac{2\pi x}{\ell} - D_{12} \alpha^2 \cos \frac{2\pi x}{\ell} \sin^2 \frac{\pi x}{\ell} + \frac{1}{4} D_{22} \alpha^4 \sin^4 \frac{\pi x}{\ell} \right) \sin^2 \frac{\pi y}{b} + D_{33} \alpha^2 \sin^2 \frac{2\pi x}{\ell} \cos^2 \frac{\pi y}{b} \right] dx dy .$$

Upon estimating the integrals and taking into consideration (1.15) and (1.16) the energy is

$$\bar{U}_b = \frac{\ell b}{\delta_4} N_{cr}^{II} \left(\bar{N}_{x0} - N_{cr}^{II} \right),$$

Or, with (1.18) in mind, we can write

$$\bar{U}_b = \frac{\ell b}{\delta_1} N_{cr}^{II} \frac{N_{x0} - N_{cr}^{II}}{\delta_4 + \ell} . \quad (1.20)$$

The midsurface deformation energy component is represented by

$$\bar{U}_p = \frac{1}{2} \int_0^L \int_0^b \left(A_{11} N_x^2 + A_{22} N_y^2 + 2A_{12} N_x N_y + A_{33} N_{xy}^2 \right) dx dy ,$$

here, equation (1.13) for stress resultants is substituted:

$$\bar{U}_p = \frac{Lb}{2\delta_1} N_{x0}^2 + \frac{t^4}{2} \int_0^\ell \int_0^b \left\{ \delta_1 \cos^2 \frac{2\pi y}{b} + \delta_2 \left(\cos^2 \frac{2\pi x}{\ell} + \frac{1}{16} \cos^2 \frac{4\pi x}{\ell} \right) + \delta_3 \alpha^4 \left[\left(\alpha^4 A_{11} + 2\alpha^2 A_{12} + A_{22} \right) \cos^2 \frac{2\pi x}{\ell} \cos^2 \frac{2\pi y}{b} + \alpha^2 A_{33} \sin^2 \frac{2\pi x}{\ell} \sin^2 \frac{2\pi y}{b} \right] \right\} dx dy .$$

Upon estimating the integrals and taking into consideration (1.16) the energy expression becomes

$$\bar{U}_p = \frac{Lb}{2\delta_4} \left[\bar{\delta}_4 \bar{N}_{x0}^2 + \bar{\ell} \left(\bar{N}_{x0} - N_{cr}^{II} \right)^2 \right],$$

or, due to (1.18), the relation (1.21) appears:

$$\bar{U}_p = \frac{Lb}{2\delta_1} \left[\frac{\bar{\delta}_4 N_{x0}^2 + \bar{\ell} \left(N_{cr}^{II} \right)^2}{\bar{\delta}_4 + \bar{\ell}} \right] . \quad (1.21)$$

Now substitute (1.20) and (1.21) in (1.19) to derive the total potential energy for the panel in state II:

$$\bar{U}^{II} = \frac{Lb}{2\delta_1} \left[N_{x0}^2 - \frac{\bar{\ell}}{\bar{\delta}_4 + \bar{\ell}} \left(N_{x0} - N_{cr}^{II} \right)^2 \right] . \quad (1.22)$$

Relations (1.4) and (1.22) should be inserted in (1.1) to obtain

$$\ell b \frac{A_{11}}{2(\bar{\delta}_4 + \bar{\ell})} \left(N_{x_0} - N_{cr}^{\Pi} \right)^2 = R. \quad (1.23)$$

We may express work R released during fracture of links between the panel and $k-1$ ribs:

$$R = \gamma_f b (k-1), \quad (1.24)$$

where γ_f is the specific work necessary to separate the panel from a rib over a unit length of the rib flange.

For the moment when the panel becomes separated from ribs, the stress resultant N_{x_0} is determined from (1.23) and (1.24):

$$N_{x_0} = N_{cr}^{\Pi} + \sqrt{\frac{k-1}{k} \left[\frac{2(\bar{\delta}_4 + \bar{\ell})\gamma_f}{a A_{11}} \right]}. \quad (1.25)$$

Both left-hand and right-hand sides in (1.25) could be undimensionalized by dividing these by the critical load $N_{cr}^* = N_{cr}^{IV}$ for buckling between ribs (refer to state IV in Fig. 1.2); the critical load is obtained in the usual way by approximating the out-of-plane displacement with the formula $w = f \sin \frac{\pi x}{a} \sin \frac{\pi y}{b}$:

$$N_{cr}^{IV} = \frac{\pi^2 D_{11}}{a^2} k_{cr}^{IV}, \quad k_{cr}^{IV} = 1 + 2\alpha_0^2 \frac{D_3}{D_{11}} + \alpha_0^4 \frac{D_{22}}{D_{11}}, \quad (1.26)$$

where

$$\alpha_0 = \frac{a}{b}, \quad 0 \leq \alpha_0 \leq \sqrt[4]{4 \frac{D_{11}}{D_{22}}}. \quad (1.27)$$

Upon these transformations, obtain

$$\bar{N} = \bar{N}^{\Pi} = \bar{N}_{cr}^{\Pi} + \sqrt{\beta^{\Pi} X}, \quad (1.28)$$

where

$$\bar{N} = \frac{N_{x_0}}{N_{cr}^{IV}}, \quad \bar{N}_{cr}^{\Pi} = \frac{N_{cr}^{\Pi}}{N_{cr}^{IV}}, \quad X = \frac{\gamma_f}{a \gamma_p}, \quad \gamma_p = \frac{1}{2} A_{11} \left(N_{cr}^{IV} \right)^2, \quad \beta^{\Pi} = \frac{k-1}{k} \left(\bar{\delta}_4 + \frac{k}{k_m} \right). \quad (1.29)$$

The γ_p variable is the specific energy that would be accumulated in a panel with a unit length, which is compressed with the stress resultant N_{cr}^{IV} ; also, the undimensionalized value X is the relative energy spent to separate the panel from a rib.

In order to determine the minimum possible value $\bar{N} = \bar{N}^{\Pi}$ we must minimize (1.28) with respect to k , where $k = 2, 3, \dots, k_m$.

Now we should analyze panel buckling with transition from state I to state III (Fig. 1.2) – that is, panel buckling with separation over the length $\ell = k a$ from $k - 1$ ribs and two spars to which the panel is attached by its side edges.

Upon the separation from spars the longitudinal edges are free. Displacement w may be expressed as,

$$w = f \sin^2 \frac{\pi x}{\ell}. \quad (1.30)$$

With links between the panel and spars broken, the panel buckles over the length ℓ , and load decreases to \overline{N}_{x0} . During transition from state I to state III the displacement Δ_x does not vary. So the panel buckling critical stress resultant is

$$N_{cr}^{III} = \frac{\pi^2 D_{11}}{a^2} k_{cr}^{III}, \quad k_{cr}^{III} = \frac{4}{k^2}. \quad (1.31)$$

Now we use analogy with theories of [5] for the angle of the tangent to the midsurface of the buckled panel in the longitudinal direction and take into account (1.30) to obtain

$$\vartheta = \theta \vartheta_{cr},$$

where

$$\theta = \sqrt{8 \frac{\overline{N}_{x0} - N_{cr}^{III}}{N_{cr}^{III}}}, \quad \vartheta_{cr} = \sin \frac{2\pi x}{\ell}.$$

To derive the displacement w , we utilize the boundary condition $\{w = 0 \text{ at } x = 0 \text{ and } x = \ell\}$:

$$w = \theta \int_0^x \vartheta_{cr} ds = \theta \frac{\ell}{\pi} \sin^2 \frac{\pi x}{\ell}.$$

This relation is compared with (1.30) to have,

$$f^2 = \frac{\ell^2}{8} \frac{\pi^2}{\ell^2} = \frac{\overline{N}_{x0} - N_{cr}^{III}}{N_{cr}^{III}}. \quad (1.32)$$

The stress resultants N_x , N_y , and N_{xy} for state III are

$$N_x = -\overline{N}_{x0}, \quad N_y = N_{xy} = 0. \quad (1.33)$$

The mutual displacement of edges $\{x = 0\}$ and $\{x = L\}$ is written with due consideration of (1.2), (1.5), (1.33), and (1.32):

$$\Delta_x = - \int_0^L \frac{\partial u}{\partial x} dx = 2\ell \frac{\overline{N}_{x0} - N_{cr}^{III}}{N_{cr}^{III}} + LA_{11} \overline{N}_{x0}. \quad (1.34)$$

The external load \bar{N}_{x0} of the buckled panel may be evaluated by using the condition $\Delta_x = \text{const}$ for the panel transition from state I to state III. With (1.3) and (1.34) in force, we have

$$\bar{N}_{x0} = \frac{\varepsilon_{cr} N_{x0} + 2\bar{\ell} N_{cr}^{III}}{\varepsilon_{cr} + 2\bar{\ell}}, \quad (1.35)$$

where

$$\varepsilon_{cr} = A_{11} N_{cr}^{III}. \quad (1.36)$$

From (1.32) and (1.35):

$$t^2 = \frac{\bar{N}_{x0} - N_{cr}^{III}}{\delta_1 (\varepsilon_{cr} + 2\bar{\ell})}. \quad (1.37)$$

The bending energy component is expressed as,

$$\bar{U}_b = \frac{b}{2} \int_0^\ell D_{11} \left(\frac{\partial^2 w}{\partial x^2} \right)^2 dx.$$

Now substitute w from (1.30) and allow for (1.36) and (1.37) to obtain

$$\bar{U}_b = \ell b \frac{A_{11}}{2} 4 N_{cr}^{III} \frac{N_{x0} - N_{cr}^{III}}{\varepsilon_{cr} + 2\bar{\ell}}. \quad (1.38)$$

The relation (1.33) is now taken into account to derive the compression energy component for the plate midsurface:

$$\bar{U}_p = \frac{b}{2} \int_0^L A_{11} N_x^2 dx.$$

Herein, we substitute stress resultants from (1.33) and (1.35):

$$\bar{U}_p = L b \frac{A_{11}}{2} \left(\frac{\varepsilon_{cr} N_{x0} + 2\bar{\ell} N_{cr}^{III}}{\varepsilon_{cr} + 2\bar{\ell}} \right)^2. \quad (1.39)$$

With relations (1.4), (1.38), and (1.39) obtained, equation (1.1) may be re-written as

$$\ell b \frac{A_{11}}{2} \frac{\varepsilon_{cr} + \bar{\ell}}{(\varepsilon_{cr} / 2 + \bar{\ell})^2} (N_{x0} - N_{cr}^{III})^2 = R.$$

Real panels are characterized with the interrelation $\varepsilon_{cr} \ll \bar{\ell}$, so

$$L b \frac{A_{11}}{2} (N_{x0} - N_{cr}^{III})^2 = R. \quad (1.40)$$

Let us decompose R into two summands:

$$R = R_f + R_r, \quad (1.41)$$

where

$$R_f = \gamma_f b (k - 1), \quad R_r = 2 \gamma_r a \cdot k, \quad (1.42)$$

γ_r is the specific energy necessary to separate the panel from a unit length of the spar.

Here, we substitute (1.41) and (1.42) in (1.40) and take into analysis that $\bar{\ell} = k / k_m$:

$$N_{x_0} = N_{cr}^{III} + \sqrt{\frac{2k}{a A_{11} k_m} \left(\frac{k-1}{k} \gamma_f + 2\alpha_0 \gamma_r \right)}. \quad (1.43)$$

Both left-hand and right-hand sides of (1.43) may be divided by the critical stress resultant $N_{cr}^* = N_{cr}^{IV}$ for panel buckling within a single bay with no separation from ribs and spars (refer to state IV in Fig. 1.2):

$$\bar{N} = \bar{N}^{III} = \bar{N}_{cr}^{III} + \sqrt{\beta^{III} X}, \quad (1.44)$$

where X corresponds to (1.29) and

$$X_r = \frac{\gamma_r}{a \gamma_p}, \quad \bar{N}_{cr}^{III} = \frac{N_{cr}^{III}}{N_{cr}^{IV}}, \quad \beta^{III} = \frac{1}{k_m} \left[k(1 + 2\alpha_0 \bar{X}_r) - 1 \right], \quad \bar{X}_r = \frac{X_r}{X}. \quad (1.45)$$

For particular values of α_0 and ratio \bar{X}_r we should determine the value of k (with $k = 1, 2, \dots, k_m$) which provides the minimum \bar{N} level.

The maximum load \bar{N} that may be carried by the panel not separating from supports (with panel parameters and link fracture energy prescribed) corresponds to the lower value among \bar{N}^{II} and \bar{N}^{III} (as provided by (1.28) and (1.44)) while assuming that $\bar{N} < 1$. Note that both (1.28) and (1.44) have been obtained under the assumption of $N_{x_0} \leq N_{cr}^{IV}$; so the relations are allowed to be united as

$$\bar{N} = \begin{cases} \bar{N}^{II} & \text{if } \bar{N}^{II} \leq \bar{N}^{III} \text{ and } N_{x_0} \leq N_{cr}^{IV}, \\ \bar{N}^{III} & \text{if } \bar{N}^{II} > \bar{N}^{III} \text{ and } N_{x_0} \leq N_{cr}^{IV}, \\ 1 & \text{if } \min(\bar{N}^{II}, \bar{N}^{III}) > 1. \end{cases} \quad (1.46)$$

Let us use X_{cr} to denote the minimum possible value of the relative link fracture energy X for links between the panel and a rib; this X_{cr} value at the X_r / X ratio specified ensures $\bar{N} = 1$ (see (1.46)), and no greater X value could increase the failure load. From (1.28), (1.44), and (1.46) we obtain

$$X_{cr} = \begin{cases} X_{cr}^{II}, & \text{if } X_{cr}^{II} \geq X_{cr}^{III} \\ X_{cr}^{III}, & \text{if } X_{cr}^{II} < X_{cr}^{III} \end{cases},$$

where

$$X_{cr}^{II} = \max_{k=2,3,\dots,k_m} \left\{ \frac{1}{\beta^{II}} \left(1 - \bar{N}_{cr}^{II} \right)^2 \right\}, \quad X_{cr}^{III} = \max_{k=1,2,\dots,k_m} \left\{ \frac{1}{\beta^{III}} \left(1 - \bar{N}_{cr}^{III} \right)^2 \right\}.$$

These formulas utilize the k values which ensure $\bar{N}_{cr}^{II} \leq 1$ and $\bar{N}_{cr}^{III} \leq 1$, respectively.

When $X \geq X_{cr}$, the panel is attached to supports strongly enough for the panel to buckle between ribs (i.e., to come to the state IV) with no separation from ribs and/or spars. Thus, the critical value X_{cr} of link fracture relative energy at \bar{X}_r prescribed is an important indicator of strength of joints between the panel and its longitudinal and transverse supports.

In particular, the present methodology may be employed to evaluate link fracture energy for a skin and the longitudinal and transverse stiffeners.

1.2. Dependence of ultimate load on panel parameters and link fracture energy available: A parametric study

In the general case an orthotropic panel may be described as a composite skin (with a thickness h and a symmetric stacking) stiffened with stringers. The material characteristics of the orthotropic skin include $E_1^0, E_2^0, G^0, \mu_1^0$, and μ_2^0 – that is, elastic and shear moduli and Poisson's ratio. Stringer parameters include the following set:

- $b_s = b / (n_s + 1)$, the stiffener spacing,
- n_s , the total number of stiffeners,
- E_s , the stiffener Young modulus,
- F_s , the stiffener cross-sectional area,
- I_s , the stiffener cross section inertia moment, and
- z_s , the distance from the stiffener cross section centroid to the skin midsurface.

For the panel the compliance cocos are

$$A_{11} = \frac{1}{E_1 h}, \quad A_{22} = \frac{1}{E_2 h}, \quad A_{12} = -\frac{\mu_1}{E_1 h} = A_{21} = -\frac{\mu_2}{E_2 h}, \quad A_{33} = \frac{1}{G h},$$

where

$$E_1 = E_1^0 (1 + r), \quad E_2 = E_2^0 \frac{1 + r}{1 + \bar{r}}, \quad \mu_1 = \mu_1^0, \quad \mu_2 = \frac{\mu_2^0}{1 + r}, \quad \mu_2^0 = \mu_1^0 \frac{E_2^0}{E_1^0},$$

$$G = G^0, \quad \bar{r} = r (1 - \mu_1^0 \mu_2^0), \quad r = \frac{E_s F_s}{E_1^0 h b_s}.$$

The panel bending stiffness is determined through skin and stringer stiffnesses as follows:

$$D_{11} = D_{11}^0 + D_{11}^*, \quad D_{22} = D_{22}^0, \quad D_3 = D_3^0 = D_{12} + 2D_{33},$$

where

$$D_{11}^0 = \frac{E_1^0 h^3}{12(1 - \mu_1^0 \mu_2^0)}, \quad D_{22}^0 = \frac{E_2^0 h^3}{12(1 - \mu_1^0 \mu_2^0)}, \quad D_{33} = D_{33}^0 = \frac{G^0 h^3}{12},$$

$$D_{11}^* = \frac{E_1^0 h}{1 - \mu_1^0 \mu_2^0} h_1^2 + \frac{E_s I_s}{b_s} + \frac{E_s F_s}{b_s} (z_s - h_1)^2, \quad D_{12} = D_{12}^0 = \frac{1}{2} (\mu_2^0 D_{11}^0 + \mu_1^0 D_{22}^0),$$

and h_1 is the distance from the skin midsurface to the centroid of the cross section of the stiffener with the neighbouring skin.

By analyzing formulas (1.28) and (1.44) it can be concluded that, with X and X_r / X specified, the value of \bar{N} (and the integer k which minimizes \bar{N}) depends on the following parameters:

$$\alpha_0, \quad k_m, \quad \frac{A_{22}}{A_{11}}, \quad \frac{A_3}{A_{11}}, \quad \frac{D_{11}}{D_{22}}, \quad \frac{D_{11}}{D_3}.$$

It is easy to write similar parameters for a plain (unstiffened) orthotropic panel:

$$\alpha_0, \quad k_m, \quad \frac{E_2^0}{E_1^0}, \quad \frac{G^0}{E_1^0}, \quad \mu_1^0.$$

In case the panel is isotropic the \bar{N} value does only depend on α_0 , k_m , and μ .

Thus, the total number of parameters influencing \bar{N} is rather large. In this connection we limit ourselves to analysis of a few typical versions that help nevertheless to detail the entire methodology.

Firstly, let us consider a 10-bay panel (with $k_m = 10$) attached to ribs and spars; assume that the rib spacing is much less than the distance between spars (here, $\alpha_0 = 0.2$). At the initiatory stage, we presume in addition that the relative strength of panel/spar links is notably greater than that of panel/rib links ($X_r / X \gg 1$) – this means that, as the load is growing, the panel may separate from ribs only. We will address three versions of panel design:

- isotropic panel,
- homogeneous orthotropic panel, and
- inhomogeneous orthotropic panel (stiffened in the longitudinal direction).

Figure 1.4 represents the dependence of \bar{N} on X for the isotropic panel in which

$$\frac{D_{11}}{D_{22}} = \frac{A_{22}}{A_{11}} = \frac{D_{11}}{D_3} = \frac{A_3}{A_{11}} = 1.$$

If the available link fracture energy X grows, the ultimate load \bar{N} gradually increases, which is accompanied with shortening of the separation zone length $\ell = k a$. For example, within the interval $\{X_{56} < X < X_{45}\}$ the panel buckles and separates from four ribs ($k=5$), whereas within the interval $\{X_{56} < X < X_{cr}\}$, from three ribs ($k=4$). When $X \geq X_{cr}$ the panel buckles between ribs and obtains the shape corresponding to state IV in Fig. 1.2. From Fig. 1.4 it is seen that the isotropic panel is characterized with $X_{cr} = 0.53$.

Figure 1.5 depicts the same kind of dependence for the homogeneous orthotropic panel (that has a composite skin with a symmetric layup and no stiffeners) in which

$$\frac{D_{11}}{D_{22}} = \frac{A_{22}}{A_{11}} = 2.87, \quad \frac{D_{11}}{D_3} = 3.64, \quad \frac{A_3}{A_{11}} = 4.63.$$

The panel dimensions are the same as in the previous example. Here, we have the critical value $X_{cr} = 0.71$, which is higher than that in the isotropic structure.

Figure 1.6 shows the « $\bar{N}-X$ » diagram for the orthotropic panel (with a composite skin and stiffeners) in which the in-plane dimensions are identical to those in previous versions; here,

$$\frac{D_{11}}{D_{22}} = 70.1, \quad \frac{A_{22}}{A_{11}} = 3.46, \quad \frac{D_{11}}{D_3} = 88.8, \quad \frac{A_3}{A_{11}} = 5.63.$$

Here, the structure has the critical value $X_{cr} = 0.77$, which is slightly higher than that in the unstiffened composite panel.

By comparing values of X_{cr} for the three versions, it is clear that increasing the longitudinal stiffness results in greater X_{cr} values.

Of interest is the dependence of X_{cr} on the relative rib spacing α_0 .

Figure 1.7 demonstrates how X_{cr} of the isotropic panel depends on α_0 ; Figures 1.8 and 1.9 show similar functions for the homogeneous composite skin and the orthotropic panel with the stiffnesses reported above.

From Figures 1.7 through 1.9 it is seen that X_{cr} notably decreases as α_0 grows.

Below, we consider the same panels but assume that these could buckle in accordance with models II and III. The ratio $X_r / X = \gamma_r / \gamma_f$ for these examples reaches various levels:

- 6.0 for the isotropic unstiffened panel,
- 4.0 for the composite unstiffened panel, and

- 3.0 for the composite stiffened panel.

Figures 1.10 through 1.12 represent relevant « $\bar{N} - X$ » diagrams. The curve corresponding to state II intersects (at a certain point $X = X_{III \rightarrow II}$) with the curve for state III. For the panel versions under consideration the X_{cr} value are on the curve corresponding to state II.

Figures 1.13 through 1.15 demonstrate the X_{cr} dependence on α_o . As for the isotropic panel the curve corresponding to state II intersects the state III curve at the point with $\alpha_o \cong 0.23$. Consequently, if the available X value is below X_{cr} , whereas $\alpha_o < 0.23$, then the buckled panel may separate from ribs only - state II. If, however, the available X value is below X_{cr} , but $\alpha_o > 0.23$, the buckled panel separates from ribs and spars - state III. And the structure with $X > X_{cr}$ buckles between ribs with no failure of links to both the ribs and spars - state IV. As for homogeneous composite and structurally orthotropic panels (with the respective X_r / X values written above) the coordinate α_o of intersection of curves corresponding to states II and III is slightly larger than that for the isotropic panel (here, $\alpha_o \cong 0.31$ and $\alpha_o \cong 0.34$, respectively).

To conclude the investigation, we carried out studies on dependence of \bar{N} on X and X_{cr} on α_o for panels with different lengths - at $k_m = 7, 8, 9, 10$.

Figure 1.16 depicts the dependence of \bar{N} on X for the isotropic panel at $\alpha_o = 0.2$. The bright circles on the curves denote panel transition from type III buckling to type II buckling.

Figure 1.17 demonstrates how X_{cr} for the same panel depends on α_o . These curves suggest that decreasing the total number of bays in the generic panel decreases X_{cr} , other things being equal. This is associated with the fact that, with the total number of bays decreased, the potential energy of the unbuckled panel portion (whose length is $L - \ell$) decreases as compared with the total energy of the entire panel upon buckling.

Figure 1.18 shows dependence of X_{cr} on α_o for the composite stiffened panel whose stiffnesses are represented in the Figure.

Figure 1.19 provides the computed results on X_{cr} as a function of the "relative stiffness capability" in the longitudinal direction - D_{11} / D_{22} ; the α_o parameter assumes certain values: 0.2, 0.25, 0.3, 0.35, and 0.4. In the case of $D_{11} / D_{22} > 20$ the parameter is seen not to influence X_{cr} .

Part 2. Fracture energy and strength of links between the multispan panel and supports: Critical values for ensuring traditional buckling with nodal lines being on the supports

Part 1 above introduced the notion of "specific link fracture energy X " for a compression-loaded multispan panel attached to supports; also, Part 1 provides analytical expressions and some parametric analyses that establish dependence of the panel failure load on X . To carry out real analyses, one should be able to determine X for particular supports and joints. There exist various designer solutions in respect of supporting elements and types of panel-to-support joints. In addition, the "panel-joint-support" system fails at its weakest point. So the link fracture energy is recommended to be determined by resorting to special experiments with real structure parts; experimenters should record

- the load-displacement diagram, « $q - \Delta$ », and
- the ultimate load q_p

(here, q is the linear density of the peeling-off load normal to the panel surface and applied to the line of joint between the panel and the support, and Δ is the displacement in the q direction). This diagram must be obtained while increasing the load q from zero to "panel-

support" link fracture. The area outlined by this diagram, $\int_0^{\Delta_p} q d\Delta$ is the equivalent to the link

fracture energy; here, Δ_p is the displacement at fracture.

However, the experimenting with real structural parts is difficult to implement for a number of reasons. In this connection we propose the method for theoretically determining the link fracture energy while assuming that the weakest point in the "panel-support" system is the joint (i.e., a bolted or riveted joint or an adhesive bond) whereas the support itself is rather stiff. If the support is a beam-like rib transferring its load to spars, then the rib deformation energy,

$$U_{b.w.} = \int_0^b \frac{M^2(q_p)}{2EJ} dy + \int_0^b \frac{\alpha Q^2(q_p)}{2GF} dy \quad (2.1)$$

can be added to the fracture energy of the joint, as this energy is released at the failure time instant. In the above equation the symbols $M(q_p)$ and $Q(q_p)$ are the bending moment and the shear force at the load q_p , respectively, and EJ and GF are the rib bending and shear stiffnesses, respectively.

Let us preliminarily address a simplified approach to bolt/rivet fracture energy, provided that the joint fails because of breakage of the rod of a bolt or rivet.

2.1. The method to evaluate link fracture energy for bolted and riveted joints. Relation to load-displacement diagram and bolt/rivet fracture load

To carry out real analyses, designers should evaluate parameters γ_f and γ_r . We suggest the method for determining these on the basis of experimentally obtained «q – Δ» diagram; here, q is the linear density of the tensile load that tears the panel off the rib/spar, and Δ is a characteristic displacement in the joint subjected to tension. The specific fracture energy (per unit length of the joint) is,

$$\gamma = \int_0^{\Delta_p} q d\Delta, \quad (2.2)$$

where Δ_p is the characteristic displacement at fracture time instant.

If the panel is attached to the supports by using bolts and/or rivets, and the fasteners fail due to rod breakage, then γ may be approximately computed on the basis of the «σ – ε» diagram for the bolt/rivet material.

Assume that the «σ – ε» diagram for tension of a bolt/rivet has the shape represented in Fig. 2.1; here, we employ the following notation: σ_{02} is the yield stress; $\varepsilon_2 = \sigma_{02}/E$; and σ_p and ε_p are the ultimate stress and the relative elongation at fracture, respectively.

With this, the rivet/bolt fracture energy and the γ value may be calculated as,

$$A = HFS_d \quad \text{and} \quad \gamma = \frac{n}{c} HFS_d, \quad (2.3)$$

where

H and F are rivet/bolt rod length and cross-sectional area, respectively,

c is the rivet/bolt spacing in a row,

n is the number of rivet/bolt rows in the joint, and

$S_d = \int_0^{\varepsilon_p} \sigma d\varepsilon$ is the area occupied by the «σ – ε» diagram; the area may be approximately

computed as,

$$S_d = \sigma_p \varepsilon_p \eta, \quad (2.4)$$

where η is the «σ – ε» diagram filling ratio:

$$\eta = \frac{1}{2} \left(1 + \frac{\sigma_{02}}{\sigma_p} - \frac{\varepsilon_2}{\varepsilon_p} \right), \quad 0.5 \leq \eta \leq 1. \quad (2.5)$$

Thus, to determine γ , we should substitute the integral (2.4) into the formula (2.3):

$$\gamma = \eta q_p \Delta_p, \quad (2.6)$$

note that

$$q_p = \frac{\sigma_p F}{c} n \quad \text{and} \quad \Delta_p = H \varepsilon_p. \quad (2.7)$$

By substituting (2.6) into (1.29) and (1.45), we obtain relative link fracture energy values X (for ribs) and X_r (for spars):

$$X = \frac{2 \eta_f q_{pf} \Delta_{pf}}{A_{11} (N_{cr}^{IV})^2}, \quad X_r = \frac{2 \eta_r q_{pr} \Delta_{pr}}{A_{11} (N_{cr}^{IV})^2}, \quad (2.8)$$

Here, q_{pf} , q_{pr} , η_f , η_r , Δ_{pf} , and Δ_{pr} are the characteristics introduced above for evaluating joints between the panel and ribs and spars, respectively.

The values X and X_r enable one to use either plots in Figs 1.10 through 1.12 or immediate computation in order to establish

- the load at failure of the compression-loaded multispan panel and
- the real buckling mode (that is, II, III, or IV).

There exists an opposite problem: one may want to ensure such a buckling surface shape between ribs that links do not fail; in this situation the condition $X \geq X_{cr}$ makes it possible to determine the required parameters of bolts and rivets, as (2.7) includes fracture characteristics σ_p and ε_p , bolt/rivet section area F , spacing c , and number of rows n .

2.2. Finite element analysis of link fracture energy for bolted joints

A joint is a system of discrete, irregular components which are in contact. A joint may fail not only because of the bolt/rivet rod breakage considered in 2.1 but also due to head separation and/or breakage of a plate/support near the bolt/rivet head. In this connection the discrete link fracture energy should be established by utilizing Finite Element Methods (FEM). The joint with the neighbouring portions of a rib and/or spar should be "dissociated" into finite elements, and for each element we must determine the stress tensor σ_{ij} and the strain tensor ε_{ij} ; the joint is assumed to be loaded with tension due to detachment of the parts. In this case the energy accumulated by the components during the system deformation to failure is described by the following expression:

$$A = \int_V \int_0^{\varepsilon_p} \sigma_{ij} d\varepsilon_{ij} dV, \quad (2.9)$$

where V is the total volume of all elements in the unit, and ε_p is the breaking strain (let us assume that the structural system is destroyed if the breaking strain is attained in at least one point).

It is obvious that the problem of establishing stresses and strains within the unit is notably nonlinear – due to two circumstances:

- the components are in a variable contact and
- materials are physically nonlinear, which is of importance in structures with heavy loads.

Each of these problems is traditionally solved by employing stepwise approximation methods, which require much more computation costs than dealing with linear problems. Here, we propose an efficient means for determining contact stresses and allowing for material nonlinearity within FEM.

Method for solving contact problems

The principal set of equations is obtained by minimizing the Lagrange energy functional and looks like this:

$$[K]\{\delta\} = \{R\}, \quad (2.10)$$

where $\{\delta\}$ is the nodal displacement vector, $\{R\}$ is the external load vector, and $[K]$ is the structure stiffness matrix. To solve the set (2.10) we must specify boundary displacement conditions for a certain part of the domain:

$$\delta = U_0 \quad (2.11)$$

Let us consider two bodies of arbitrary shapes (i and j are indices to identify the relevant bodies) in the Cartesian coordinate system OXY (Fig. 2.2).

Let S_{ic} and S_{jc} be the assumed surfaces of contact, i.e., those portions of the bodies i and j that can interact during loading. The surface S_{ic} at every point C_{ik} (k is a point number, $k=1, 2, \dots$) has an outward normal n_{ik} . Points C_{ik} and C_{jk} having identical second indices will hereafter be referred to as conjugate points if these could establish mutual contact. As noted in [6], whether points are conjugate can only be determined with a fair degree of accuracy and prior to solving the problem if the pattern of contact deformation is obvious and the bodies have

rather simple geometries. If it is not the case, the contact area will be outlined by employing an algorithm based on criteria of mutual nonpenetration of bodies.

Introduce radius vectors r_{oi} and r_{oj} to identify initial positions of the points C_{ik} and C_{jk} , respectively (Fig. 2.2). After loading, positions of these points in the three-dimensional space will be defined by the relations,

$$\{r_{ik}\} = \{r_{oi}\} + \{\delta_{ik}\}, \quad \{r_{jk}\} = \{r_{oj}\} + \{\delta_{jk}\}, \quad (2.12)$$

where $\{\delta_{ik}\}$ and $\{\delta_{jk}\}$ are displacement vectors of the conjugate points of the i -th and j -th bodies. The criterion of contact of the points C_{ik} and C_{jk} can be written as,

$$\left(\{r_{ik}\} - \{r_{jk}\} \right) \{n_{ik}\} = 0 \Big|_{C_{ik} \in S_{ic}}. \quad (2.13)$$

After considering equation (2.12), from equation (2.13) we obtain the compatibility condition:

$$\left(\{r_{ik}\} - \{r_{jk}\} \right) \{n_{ik}\} = \left(\{\delta_{jk}\} - \{\delta_{ik}\} \right) \{n_{ik}\} \Big|_{C_{ik} \in S_{ic}}. \quad (2.14)$$

For conjugate noncontacting points the following condition should hold:

$$\left(\{r_{ik}\} - \{r_{jk}\} \right) \{n_{ik}\} \leq 0 \Big|_{C_{ik} \in S_{ic}}, \quad (2.15)$$

which, in its essence, expresses the condition of mutual nonpenetration of bodies. In the projection on the normal n_{ik} , the condition (2.14) becomes

$$\delta_{ik}^{(n)} + \delta_o^{(n)} = \delta_{jk}^{(n)}, \quad (2.16)$$

where $\delta_{ik}^{(n)}$ and $\delta_{jk}^{(n)}$ are displacements of conjugate points of the bodies i and j along the outward normal; $\delta_o^{(n)}$ is the initial (positive or negative) interference between the conjugate points as measured along the normal n_{ik} . The equations of equilibrium of isolated bodies i and j (with no contact between these) in block matrix notation are

$$\begin{bmatrix} K_{i11} & K_{i12} \\ K_{i21} & K_{i22} \end{bmatrix} \begin{Bmatrix} \delta_{i1} \\ \delta_{i2} \end{Bmatrix} = \begin{Bmatrix} P_i \\ Q_i \end{Bmatrix}, \quad \begin{bmatrix} K_{j11} & K_{j12} \\ K_{j21} & K_{j22} \end{bmatrix} \begin{Bmatrix} \delta_{j1} \\ \delta_{j2} \end{Bmatrix} = \begin{Bmatrix} P_j \\ Q_j \end{Bmatrix}, \quad (2.17)$$

where

δ_{i1} and δ_{j1} are displacements of nodes (on the bodies i and j , respectively), that do not contact mutually,

δ_{i2} and δ_{j2} are displacements of nodes which contact one the other,

P_i and P_j are prescribed external loads, and

Q_i and Q_j are contact forces to be found.

Now we resort to the Gaussian elimination procedure for block matrices to describe unknown displacements of contact nodes:

$$[K_i^*]\{\delta_i\} = \{R_i^*\}, \quad [K_j^*]\{\delta_j\} = \{R_j^*\}, \quad (2.18)$$

where

$$[K_i^*] = [K_{i22} - K_{i21}K_{i11}^{-1}K_{i12}], \quad [K_j^*] = [K_{j22} - K_{j21}K_{j11}^{-1}K_{j12}], \quad (2.19)$$

$$[R_i^*] = [Q_i - K_{i12}K_{i11}^{-1}P_i], \quad [R_j^*] = [Q_j - K_{j12}K_{j11}^{-1}P_j].$$

Assume that the conjugate (k-th) nodes of the i-th and j-th bodies are interrelated in a local coordinate system:

$$[\gamma] \begin{Bmatrix} \delta_{ik} \\ \delta_{jk} \end{Bmatrix} = \begin{Bmatrix} Q_{ik} \\ Q_{jk} \end{Bmatrix}, \quad (2.20)$$

where

$$[\gamma] = \begin{bmatrix} [C] & -[C] \\ -[C] & [C] \end{bmatrix}, \quad (2.21)$$

Q_{ik} and Q_{jk} are the contact forces applied to the conjugate points,

$$[C] = \begin{bmatrix} C_n & 0 \\ 0 & C_\xi \end{bmatrix} \text{ in two-dimensional problems,}$$

$$[C] = \begin{bmatrix} C_n & 0 & 0 \\ 0 & C_\xi & 0 \\ 0 & 0 & C_\eta \end{bmatrix} \text{ in three-dimensional problems, and} \quad (2.22)$$

C_n , C_ξ , and C_η are link stiffnesses along the local coordinate system axes n , ξ , and η , respectively.

Let us introduce $[\lambda]$, the direction cosine matrix relating the local coordinate system (n , ξ , η) to the global one (x , y , z). Expressions (2.18) and (2.20) should be summed up to produce the equilibrium equations for the bodies in contact:

$$\begin{bmatrix} [K_i^*] + [\gamma^0] & -[\gamma^0] \\ -[\gamma^0] & [K_j^*] + [\gamma^0] \end{bmatrix} \begin{Bmatrix} \delta_i \\ \delta_j \end{Bmatrix} = \begin{Bmatrix} R_i^* \\ R_j^* \end{Bmatrix}. \quad (2.23)$$

Values in the $[\gamma^0]$ matrix characterize link stiffnesses in the general coordinate system:

$$[\gamma_{kij}^0] = [\lambda_{kij}]^T [C] [\lambda_{kij}]. \quad (2.24)$$

If the i -th body has interference, $\{\delta_o\}$, the right-hand side of the first equation in (2.19) should be complemented with the load summand

$$\{R_o\} = [K_i] \{\delta_o\}. \quad (2.25)$$

In case the bodies are not in contact, we obtain $[\gamma^0] \equiv 0$, and the formula (2.23) is rewritten as,

$$\begin{bmatrix} [K_i^*] & 0 \\ 0 & [K_j^*] \end{bmatrix} \begin{Bmatrix} \{\delta_i\} \\ \{\delta_j\} \end{Bmatrix} = \begin{Bmatrix} \begin{bmatrix} -K_{i12} & K_{i11}^{-1} & P_i \end{bmatrix} \\ \begin{bmatrix} -K_{j12} & K_{j11}^{-1} & P_j \end{bmatrix} \end{Bmatrix}. \quad (2.26)$$

The latter system for unknowns $\{\delta_i\}$ and $\{\delta_j\}$ may be solved immediately. But when there occurs a contact, the system (2.23) is to be solved using the following algorithm

1. Specify the contact nodes and their stiffness matrices $[C_{ik}]$.
2. Compute the direction cosine matrix $[\lambda]$ for the contact nodes.
3. Calculate the substructure stiffness matrices and right-hand side vectors – in accordance with (2.18).
4. Use (2.18) to derive equilibrium equations (2.19) for contact points, by utilizing the Gaussian elimination procedure.

5. Use (2.17) to determine along-the-normal interference δ_R between nodes:

$$\delta_{Rk} = \delta_{jk}^n - \delta_{ik}^n - \delta_{ok}$$

6. Find the forces R applied to the body i due to the interference δ_{Rk} :

$$\{R_i\} = [K_i] \{\delta_{Rk}\};$$

add the forces to the external load vector of the body.

7. Utilize expressions (2.24) in order to transform link stiffness matrices into the global coordinate system; add these to the structural stiffness matrix (2.23).

8. From the relation (2.23) determine the contact node displacement vectors $\{\delta_i\}$ and $\{\delta_j\}$.

9. Use (2.22) to compute contact force components along normals:

$$Q_k = C_k \lambda (\delta_{ik} - \delta_{jk}). \quad (2.27)$$

10. Check up the nonpenetration condition (2.16) being met. If yes, go to item 11 below; otherwise, repeat the analysis starting from item 5.

11. Terminate the iterations and calculate stresses by employing usual FEM relations.

Allowance for materials plasticity

If at least one component in the joint behaves nonlinearly, the contact problem is much more difficult to solve. To describe physical nonlinearity, we use the strain theory of [7].

The problem is solved under the assumption that the structural displacement are small in comparison with overall dimensions. To outline the contact area, the above algorithm is involved. The coefficients K_i^* of the equilibrium system (2.23) for the interacting elements:

$$\begin{bmatrix} [K_i^*(\delta)] + [\gamma^0] & -[\gamma^0] \\ -[\gamma^0] & [K_j^*(\delta)] + [\gamma^0] \end{bmatrix} \begin{Bmatrix} \delta_i \\ \delta_j \end{Bmatrix} = \begin{Bmatrix} R_i^* \\ R_j^* \end{Bmatrix} \quad (2.28)$$

become dependent on nodal displacements; so these should be determined by resorting to a successive approximation procedure in couple with the stepwise (incremental) loading method.

The algorithm for treating the elastic-plastic contact problem has been detailed in [8]. To improve iterations for outlining the plastic deformation zones, we utilize the secant modulus E_s correction approach similar to the Reference [9] overrelaxation method for linear algebraic systems. The correction is implemented as follows:

$$E_{si}^* = E_{si} + \omega (E_{si+1} - E_{si}),$$

where i is the plasticity iteration number and ω is the relaxation factor which is varied within the iterative cycle:

$$\omega = 1 + \Delta\omega / i^\alpha. \quad (2.29)$$

To define an optimum ω value, additional numerical experiments have been mounted for various problems. The parameter $\Delta\omega$ involved with (2.29) was changed from 0 to 0.8, whereas α was specified to be from 0.5 to 4.0. Iterations were terminated when a relative error had been less than 0.005.

It turned out that the minimum number of iterations is required in most problems when $\Delta\omega = 0.6$ and $\alpha = 2.0$. These values were utilized to solve the problems reported here.

Example problems

To improve (and approve) the present method for solving contact deformation problems, we analyzed stresses and strains in the bolted joint model that was studied in experiments with optical polarization devices, as described in [10]. A schematic of the bolt and the load application may be seen in Fig. 2.3.

The flat models of bolts were manufactured out of 4.2-mm thick plates of the optically active material, OASO. The bolt model 1 was placed on a support model 2 (made of acrylic plastic) which was on the bar 3 of the polariscope load application frame. All test models have an identical width of the cylindrical part: $d=24$ mm. The head/rod fillet radius R is 1.2 mm. The matching surface of the support 2 at the fillet has a chamfered edge measuring 2 by 2 mm.

The left-hand side of Fig. 2.4 depicts the finite-element model of bolt 1, support 2, and bar 3. The right-hand side of this Figure demonstrates deformed bolt rod and head after the force P had been applied.

Figure 2.5 represents equal shear stress lines for the tensile load $P=40$ kg. Shown to the left are lines obtained theoretically, and to the right, the pattern got by experimenters. These pictures are easy to compare to conclude that finite element analyses and experimental data converge well in both the pattern and amplitudes of maximum shear stresses.

Figure 2.6 represents theoretical variation of the stress concentration factor $K = \sigma_1 / \sigma_{nom}$ at points A and B, depending on the relative bolt head height h/d ; here, $\sigma_{nom} = P/(td)$ and σ_1 is the principal tensile stress at a point. In the Figure we provide experimental data for $h/d = 0.4, 0.5,$ and 0.6 . The most severe stress appears at the point B – on the fillet between the bolt rod and head. Therefore, it is at this point where the primary failure should be expected to occur; at a higher load the bolt head will be broken.

Consider an additional example: the problem on a cylindrical fitting (see Fig. 2.7a) loaded with tensile force $P=6000$ kg through two bolts. The FE model of the structure is depicted in Fig. 2.7b; it includes simplex axisymmetric finite elements. The total number of unknown displacements is 1298. When solving the contact problem, we considered 44 unknown displacements over the zone where the bolt interacts with the fitting (refer to Fig. 2.7a). Computed results are compared with experimental data obtained by strain gaging during tests.

Figure 2.7c demonstrates axial stress profiles over the external and internal surfaces of the cylinder. Points show the experimentally obtained values. The theory and experiment may be regarded as converging well.

Computing the link fracture energy

The link fracture energy can be determined by using (2.9). Integrals in (2.9) may be estimated by the following procedure. The external load is subdivided into a number of increments. As the load grows, each element in the unit is evaluated in what concerns stress and strain tensor components; their algebraic products are summed up for each increment by utilizing the trapezoidal technique. The volume integral is the sum over all elements of the joint.

Let us address tension of an aluminum bolt whose dimensions are represented in Fig. 2.8. The bolt material has the following characteristics: $E=7200$ kg/sq.mm, ultimate stress $\sigma_p=38$ kg/sq.mm, assumed yield limit $\sigma_{02}=24$ kg/sq.mm, and elongation at rupture, $\varepsilon_p=0.1$.

The tensile « $\sigma - \varepsilon$ » diagram of the material (see Fig. 2.1) is modeled by two straight lines: the first line approximates elastic bolt behavior, whereas the second line runs from the assumed yield limit point to the ultimate state point to approximate behavior of materials in the case of notable plastic deformation.

Figure 2.8 depicts dependence of bolt fracture energy on stress σ . We represent three versions. In the first version the bolt head rests on the support (b) manufactured of the same material. In the second version the head is in contact with an absolutely rigid support (c). In the third case we consider the bolt rod only. The analytical model for the joint under consideration is similar to the one demonstrated in Fig. 2.4 – except for the fact that, instead of flat (two-dimensional) finite elements, we used axisymmetric ones. Established as a failure criterion is the strain intensity $\varepsilon_p=0.1$. In Fig. 2.8 it is seen that the link fracture energy (symbolized with crossed squares) is slightly greater for the bolt contacting with the deformable support (1), than the value for the bolt resting on the rigid support (2). However, link fracture energy for the two versions is much less than that for the separated bolt rod (3); this is so due to the considerable stress/strain concentration at the bolt head-to-rod fillet.

Now address the second example: a skin 2 attached to a rib or spar 3 by a single-row screw joint; one of the screws 1 is depicted in Fig. 2.9. The skin thickness is 6 mm, the screw diameter is 8 mm, and the screw rod length is 20 mm.

When computing, we assumed that the rib/spar 3 is made of aluminum alloy, the screw is made of either steel or aluminum alloy; the steel has $E=21.000$ kg/sq.mm, $\sigma_p=60$ kg/sq.mm, $\sigma_{02}=40$ kg/sq.mm, and $\varepsilon_p=0.1$. The skin is made of aluminum alloy in the first version, and of a composite material in the second version. The composite skin includes 24 layers each 0.25 mm thick. A substack of 4 layers has a quasi-isotropic layup (see [11]): $[0, +45, -45, 90]$.

Characteristics of a layer may be seen in the mid-column of Table 2.1; the subscript 1 designates the fiber direction, and the subscript 2, the transverse direction; p stands for tensile load, and c is for compression. Characteristics of the entire stack are reported in the rightmost column of Table 2.1.

Table 2.1

	Layer data kg/sq.mm	Stack data kg/sq.mm
E_1	13000	5200
E_2	700	5200
G_{12}	590	2000
μ_{12}	0.36	0.29
σ_{1p}	153	51
σ_{2p}	3.4	51
σ_{1c}	120	40
σ_{2c}	3.4	40
τ_{12s}	6.0	30

The metallic materials (that is, steel and aluminum alloy) are assumed to become broken when the strain reaches its limit; for the composite material (whose fibers and matrix behave linearly to failure) we use the Tsai criterion from [12]:

$$\frac{\sigma_1^2}{S_1^2} - \frac{\sigma_1\sigma_2}{S_1^2} + \frac{\sigma_2^2}{S_2^2} + \frac{\tau_{12}^2}{S^2} = 1$$

where $S = \tau_{12s}$ is the limiting shear stress, and S_1 and S_2 are the ultimate normal stresses along and transverse to fibers, respectively:

$$S_1 = \begin{cases} \sigma_{1p} & \text{at } \sigma_1 \geq 0, \\ \sigma_{1c} & \text{at } \sigma_1 < 0, \end{cases} \quad S_2 = \begin{cases} \sigma_{2p} & \text{at } \sigma_2 \geq 0, \\ \sigma_{2c} & \text{at } \sigma_2 < 0. \end{cases}$$

Mechanical properties of the quasi-isotropic plate are obtained by using the Tsai method in [13].

Figure 2.10 demonstrates the deformed model (composed of axisymmetric finite elements). Figure 2.11 represents dependence of link fracture energy on the force P (which is calculated by integrating the distributed load p over the skin surface area).

From Fig. 2.11 it is clear that link fracture energy for the aluminum skin and the steel screw (b) is approximately twice that for the structure with an aluminum screw (a). Failure mode implemented is also depending on the screw material: the aluminum screw fails due to head separation, whereas the steel screw survives the skin.

The composite skin (represented by lines c and d) gets broken at the screw head when the separation force is at a rather low level. The fracture energy in this structure may be increased to the line b by resorting to usual designing solutions (detailed, for example, in [14]): increasing the screw head diameter, increasing the plate thickness around the joint area, etc.

2.3. Establishing parameters necessary to ensure a specified panel-to-support link strength

Consider panel separation from support in case the support (rib) deformation energy is comparable with the link fracture energy for a bolted or riveted joint. The work for separating the panel from a rib may be written as,

$$\gamma_f = \gamma_{pf} + \gamma_{bf}, \quad (2.30)$$

where γ_{pf} is the specific work of breaking the fasteners between the panel and the rib (the work is referred to a unit length of the rib flange) and γ_{bf} is the specific potential energy of rib deformation at the panel separation instant.

We can model the rib as a beam simply supported by spars at edges $\{y=0\}$ and $\{y=b\}$. At the moment which immediately precedes the panel separation from the rib, the latter is loaded with a uniformly distributed transverse force q_p . The rib deformation potential energy U_{bf} is computed by using (2.1) where

$$M = \frac{q_p}{2}(y^2 - yb), \quad Q = \frac{q_p}{2}(2y - b), \quad (2.31)$$

α_f is the coefficient depending on the rib cross-section shape; the coefficient may be assumed to be equal to 1.0 for a web-like rib.

By substituting (2.31) into (2.1) and integrating, we obtain the following expression that relates the specific potential energy $\gamma_{bf} = U_{bf}/b$ to the load q_p :

$$\gamma_{bf} = c_{bf} q_p^2 \quad (2.32)$$

where

$$c_{bf} = \frac{b^4}{240(EJ)_f} \left[1 + \frac{10}{b^2} \frac{(EJ)_f}{(GF_w)_f} \right]. \quad (2.33)$$

The coefficient c_{bf} quantifies the rib compliance under in-plane bending and shear.

The specific fracture work (referred to a unit length of the joint) can be written as follows:

$$\gamma_{pf} = c_{pf} q_p^2 \tag{2.34}$$

The coefficient c_{pf} quantifies the compliance of fasteners between the panel and the rib when loaded to failure. A particular expression for c_{pf} depends on both the panel/rib joint type and the failure mode. For example, if a panel is attached to supports by bolts or rivets and if a bolt or rivet is destroyed due to breakage of the rod, then, in accordance with (2.6) and (2.7), we obtain

$$c_{pf} = \frac{\eta_f c_f H_f}{n_f F_{pf} E_{spf}} \tag{2.35}$$

Here, $E_{spf} = \sigma_{pf} / \epsilon_{pf}$; σ_{pf} and ϵ_{pf} are respective values of fasteners at failure; F_{pf} is the bolt or rivet cross-sectional area; and c_f and n_f are the fastener spacing and the number of fastener rows, respectively.

However, fracture may be because of bolt head breakage and/or skin tear at the bolt head; in these situations the c_{pf} coefficient can be computed on the basis of data from finite-element analyses, similar to those in Figs 2.8 and 2.11.

With (1.29) derived, we have

$$\gamma_f = \frac{1}{2} a A_{11} (N_{cr}^{IV})^2 X$$

Upon substitution of (2.30), (2.32), and (2.34), the relation (2.36) between the failure load \bar{q}_p and the link fracture energy X appears:

$$q_p = \sqrt{X/c} \tag{2.36}$$

in which

$$\bar{c} = \bar{c}_{pf} + \bar{c}_{bf}, \quad \bar{c}_{pf} = \frac{2c_{pf}}{aA_{11}}, \quad \bar{c}_{bf} = \frac{2c_{bf}}{aA_{11}} \tag{2.37}$$

If one knows parameters of the rib and fasteners (that is, \bar{c} is known) the formula (2.36) can be utilized to calculate the relative per-unit-length load \bar{q}_p applied by the panel to the rib through the fasteners.

In accordance with (1.28) and (1.44), the panel coming from state I into state S (with S being either II or III) is loaded with the compressive stress resultant

$$\bar{N} = \bar{N}_{cr}^S + \sqrt{\beta^S X}$$

from here and (2.36), the expression is,

$$\bar{N} = \bar{N}_{cr}^S + \bar{q}_p \sqrt{c \beta^S} \tag{2.38}$$

Figure 2.12 represents « $\bar{N} - \bar{q}_p$ » diagrams for three versions of the stiffened panel in which the skin has the following characteristics:

$$\frac{D_{11}^0}{D_{22}^0} = \frac{A_{22}^0}{A_{11}^0} = 2.78, \quad \frac{D_{11}^0}{D_3^0} = 3.64, \quad \frac{A_3^0}{A_{11}^0} = 4.63,$$

the three panels have identical values of bending stiffness ratio $D_{11}/D_{22} = 70$ and coefficients $\alpha_o = 0.3$ and $\bar{c} = 150$; whereas, the panels differ in the ratio A_{22}/A_{11} :

$$\frac{A_{22}}{A_{11}} = 3.44, 4.30, 5.72.$$

Diagrams in Fig. 2.12 suggest that if the longitudinal stiffness of the panel stringers is increased, then a particular \bar{N} value (that is a minimum relative load which separates the panel from ribs) takes place at a lower load \bar{q}_p applied to the panel/rib fasteners.

Upon computing the available \bar{q}_p values the plots in Fig. 2.12 can be employed to determine whether the panel separates from ribs under the compressive load. If $\bar{q}_p < (\bar{q}_p)_{cr}$ then the joint will become broken at a load $N < N_{cr}^{IV}$. However, if $\bar{q}_p \geq (\bar{q}_p)_{cr}$ then the panel buckles between ribs at $N = N_{cr}^{IV}$.

If one would specify rib and fastener parameters which ensure the panel to buckle between ribs, then the parameter \bar{c} should be determined from the condition $\bar{q}_p \geq (\bar{q}_p)_{cr}$. Let us consider now the dependence of $(\bar{q}_p)_{cr}$ on some of the panel parameters.

Compute $X = X_{cr}$ by using (1.47) and (1.48) and substitute the value into (2.36) to derive the dependence of critical $(\bar{q}_p)_{cr}$ values on α_o for the panel concept versions involved; see Fig. 2.13. For each value of A_{22}/A_{11} within the interval $\{0.3 \leq \alpha_o \leq 0.45\}$ the $(\bar{q}_p)_{cr}$ variable does only slightly vary with α_o .

A similar kind of picture for $(\bar{q}_p)_{cr}$ as a function of D_{11}/D_{22} for the above values of A_{22}/A_{11} , $\alpha_o = 0.3$, and $\bar{c} = 150$ may be seen in Fig. 2.14. It is clear that $(\bar{q}_p)_{cr}$ does not almost depend on D_{11}/D_{22} when this ratio is above 50. This fact allows us to derive a unified

relation between $\left(\bar{q}_p\right)_{cr}$ and relative compliance \bar{c} of the panel-to-rib joint for $\alpha_o \geq 0.3$ and $D_{11}/D_{22} \geq 50$; the relation is demonstrated in Fig. 2.15.

There exists a really essential interval of variation of the relative panel-to-rib joint compliance: $100 \leq \bar{c} \leq 400$; here, the critical value of the relative failure load $\left(\bar{q}_p\right)_{cr}$ varies from 0.04 to 0.08 – this means that the panel-to-rib joint will fail under a load exceeding 4% - 8% of the critical compressive load \bar{N}_{cr}^{IV} ; note also that the stiffer the rib, the higher the failure load $\left(\bar{q}_p\right)_{cr}$ and the stronger the fasteners must be.

The function depicted in Fig. 2.15 makes it possible to specify parameters of usual ribs and fasteners so as to ensure the panel to buckle between ribs without breaking the joint.

CONCLUSION

The NCC-1-233 programme (in Appendix 5) dated September 15, 1998, has been the basis for the investigation of how compression-loaded multibay panels manufactured of composite materials buckle upon failure of joints with supporting elements.

The following principal results should be noticed here:

- a new method for studying the buckling of a multibay stiffened panel made of composites is proposed; it allows for destruction of panel joints with transverse and longitudinal supports in the course of buckling;
- the solution to the problem is derived; parametric research on failure load dependence on available link fracture energy and other panel parameters has been conducted;
- notions of critical link fracture energy and link strength for a multibay panel are introduced; the critical values outline the domain within which the panel buckles with nodal lines being on supports;
- techniques to compute the link fracture energy for some types of joint are proposed;
- a relation of link fracture energy to the load diagram and failure load of the joint is established; and
- a methodology for calculating the support/fastener parameters necessary to ensure a strong joint between the panel and supports is presented; usual web-like ribs and fasteners are shown to be necessarily designed so as to carry a load which is 4% to 8% of the longitudinal compressive critical force for the panel.

The present study method makes it also possible to solve the following problems of practical interest: how the compression-loaded composite panel buckles upon local separation of stiffeners from the panel and how strong the joint between the skin and stiffeners should be for the separation not to occur before the general buckling takes place.

By proceeding in a similar way, the problem of compression-loaded sandwich panel buckling with separation of the composite skin from the core over a certain (local) portion can be solved.

Efforts including solution of these and some related problems may be a continuation of the composites study programme within cooperation between NASA and TsAGI.

LITERATURE

1. Zamula G.N., Kut'inov V.F., Vasil'yev V.V., Grishin V.I., Ierusalimsky K.M., Azikov N.S., Begeyev T.K. Composite panel postbuckling behavior and general model of joints in composite structures, Moscow, TsAGI-MATI, 1996.
2. Zamula G.N., Ierusalimsky K.M., Kalmykova G.S., Fomin V.P., Analyzing the effect of skin postbuckling on general stresses, strain and stability of composite structures, Moscow, TsAGI, 1998.
3. Polilov A.N., Rabotnov Yu.N., Propagation of delamination in compression-loaded composite materials. – Izvestiya Akademii Nauk SSSR, Mekhanika Tvyordogo Tela (Solid Mechanics), Moscow, 1983, no. 4, pp. 166-171.
4. Vol'mir A.S., Elastic plates and shells. - GITTL, Moscow, 1956.
5. Alfutov N.A., Theories for analyzing stability of elastic systems. – Mashinostroyeniye, Moscow, 1991.
6. Iosilevich G.B. Concentration of stresses and strains in machine parts. – Mashinostroyeniye, Moscow, 1981.
7. Ushakov B.N., Dashirabdanov V.D., Dunayev V.V., The use of optic beam polarization methods for evaluating stresses in bolted joints with interference. – Izvestiya vuzov, Mashinostroyeniye, Moscow, 1983, no. 8, pp. 14-18.
8. Birger I.A., Mavlyutov R.R., Materials resistance science. - Nauka, Moscow, 1986.
10. Vazov V., Forsyth D., Finite difference methods for solving differential equations with partial derivatives. – IIL, Moscow, 1963.
11. Lekhnitsky S.G. Theory of elasticity for anisotropic bodies. – Nauka, Moscow, 1977.
13. Andrienko V.M., Sukhobokova G.P., Computing the strength values of multilayered inelastic composites. - Trudy TsAGI, issue 1570, 1975.
14. Tsarakhov Yu.S., Constructing the joints in composite aircraft structures. – MFTI Publishing Office, Moscow, 1982.

APPENDIX

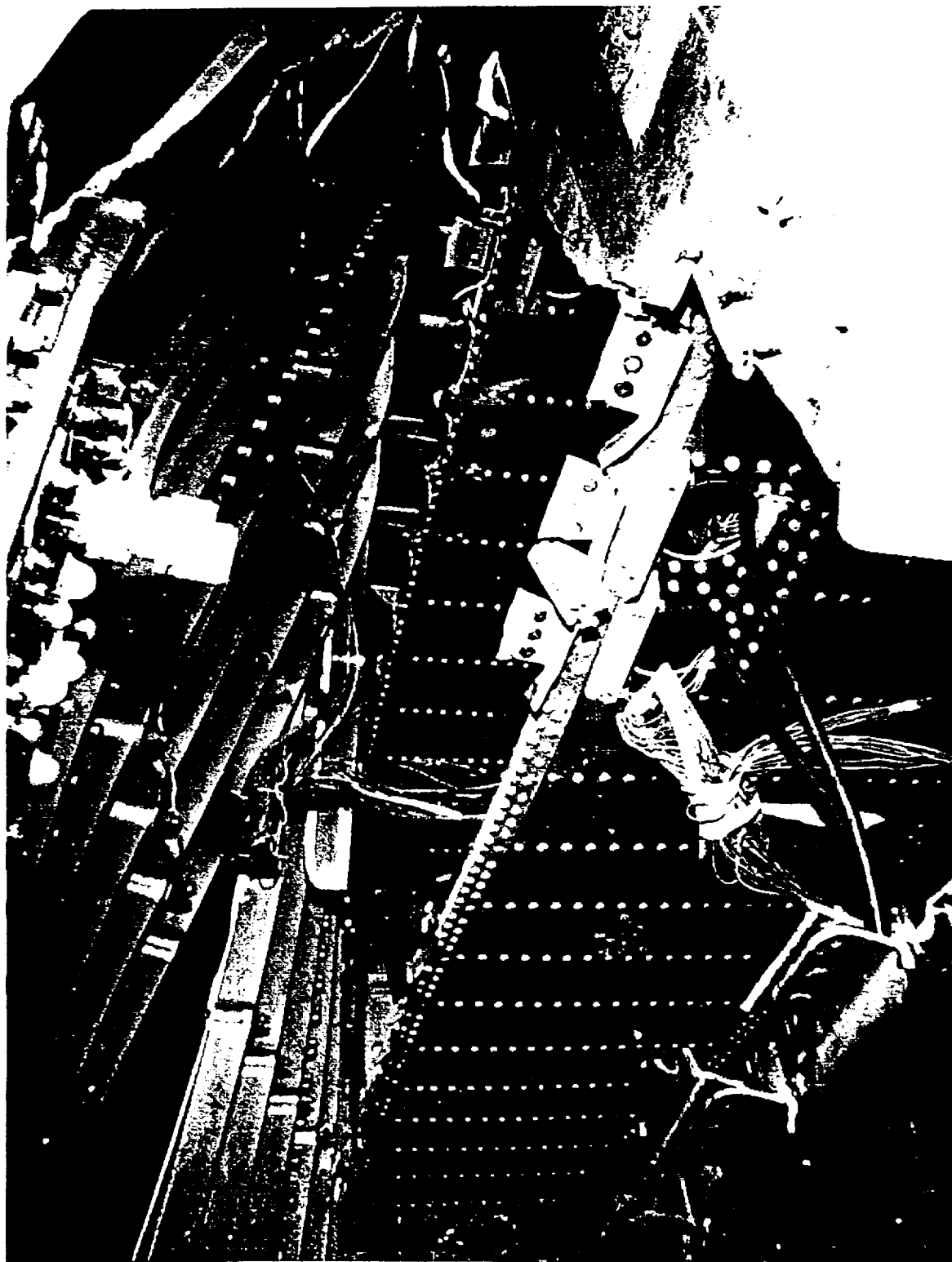


Fig. 0.1

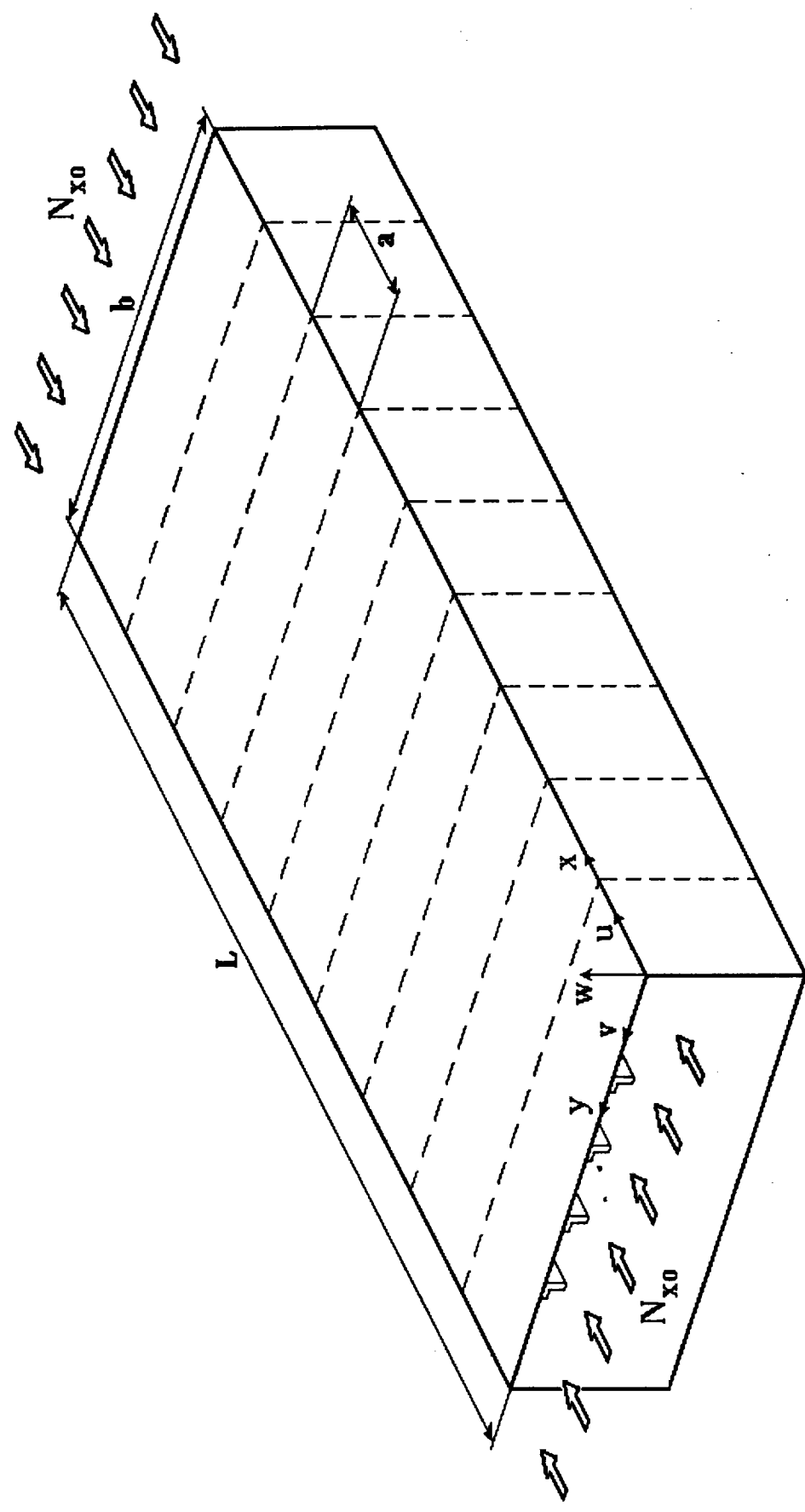


Fig 1.1

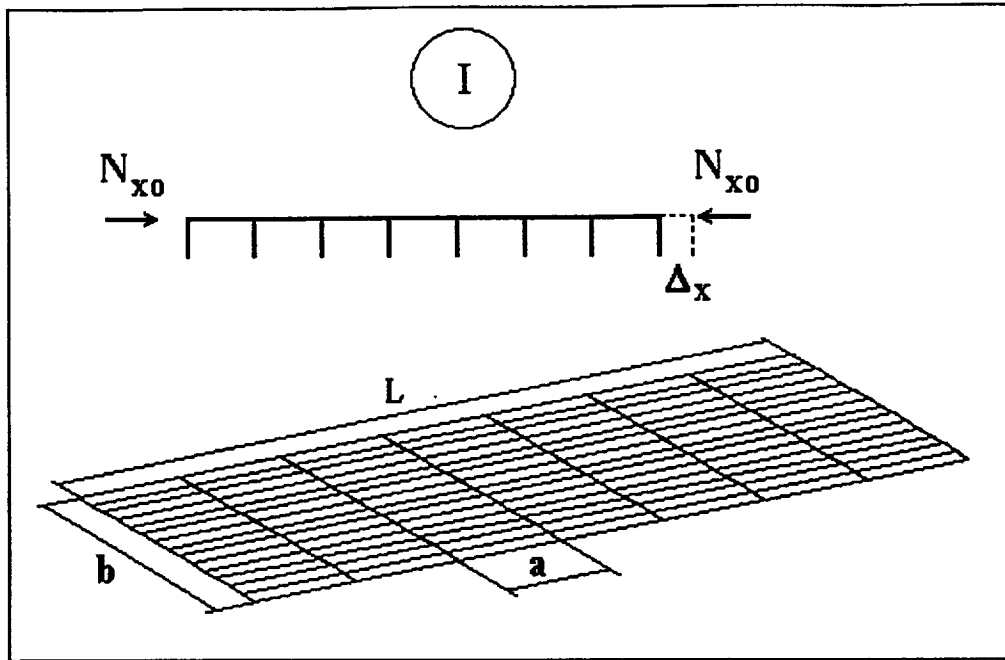


Fig. 1.2.a

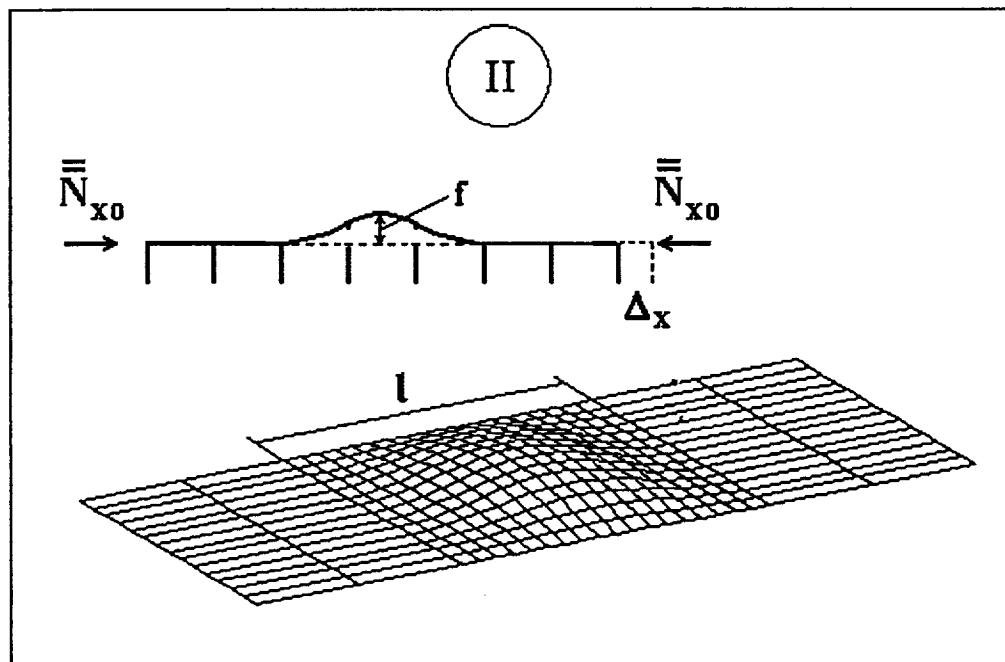


Fig. 1.2.b

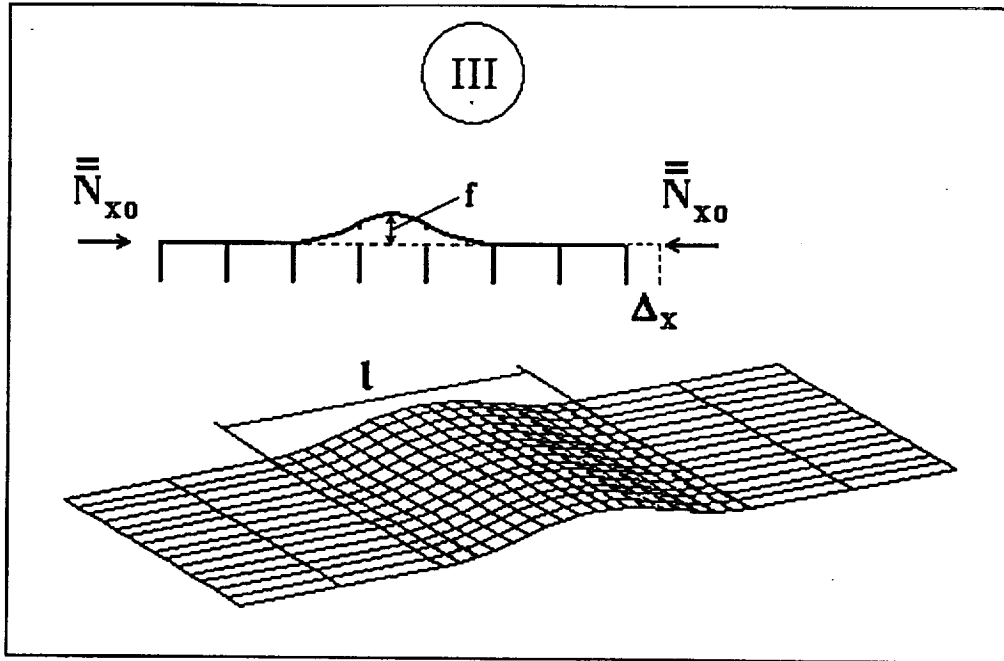


Fig. 1.2.c

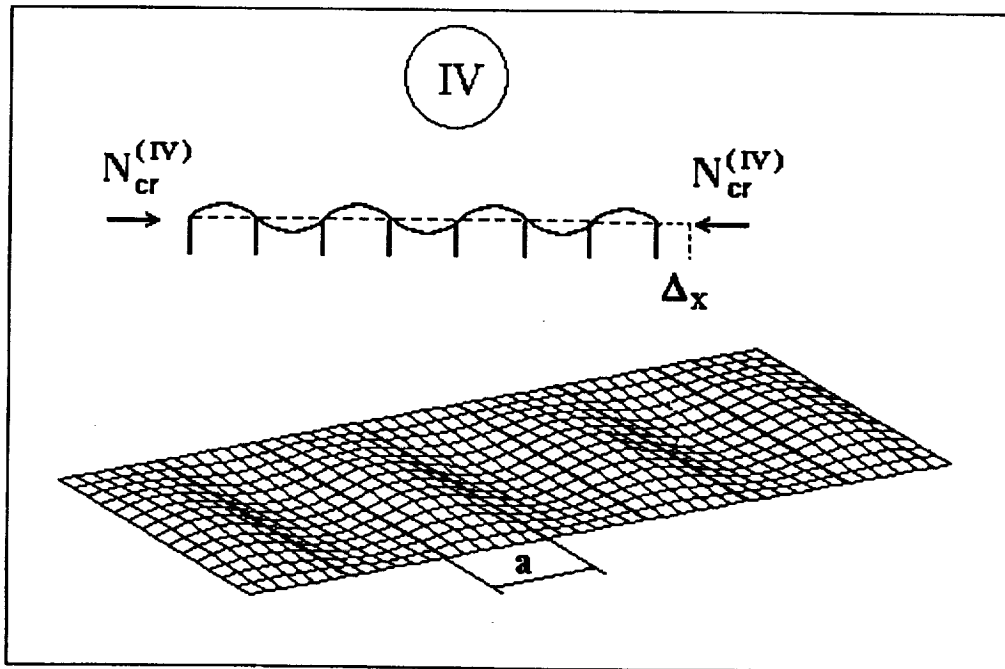


Fig. 1.2.d

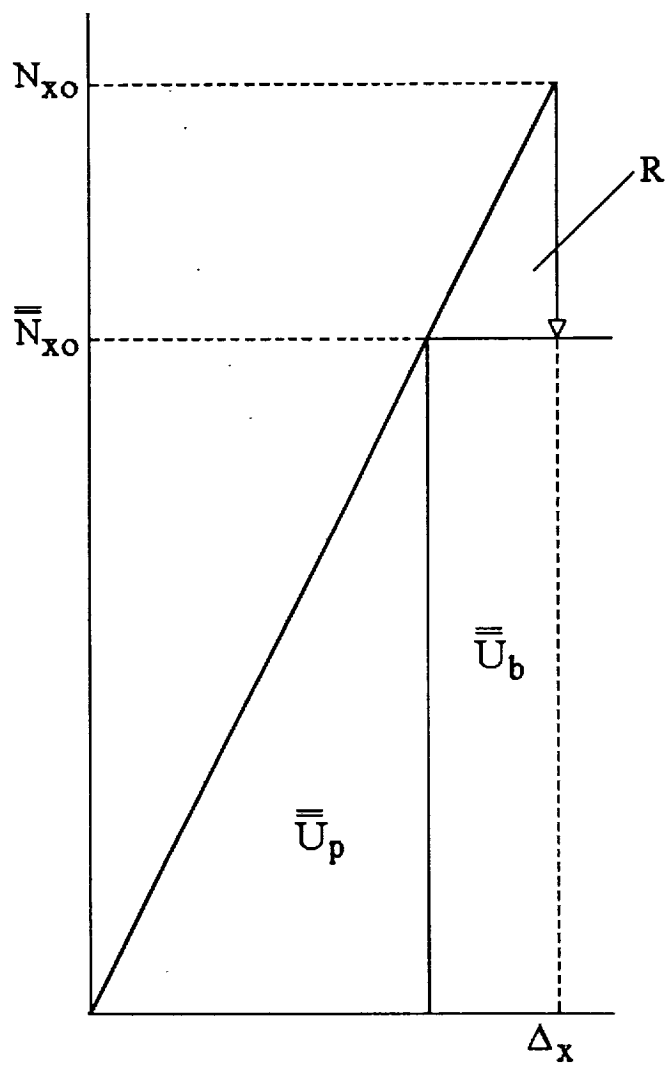


Fig. 1.3

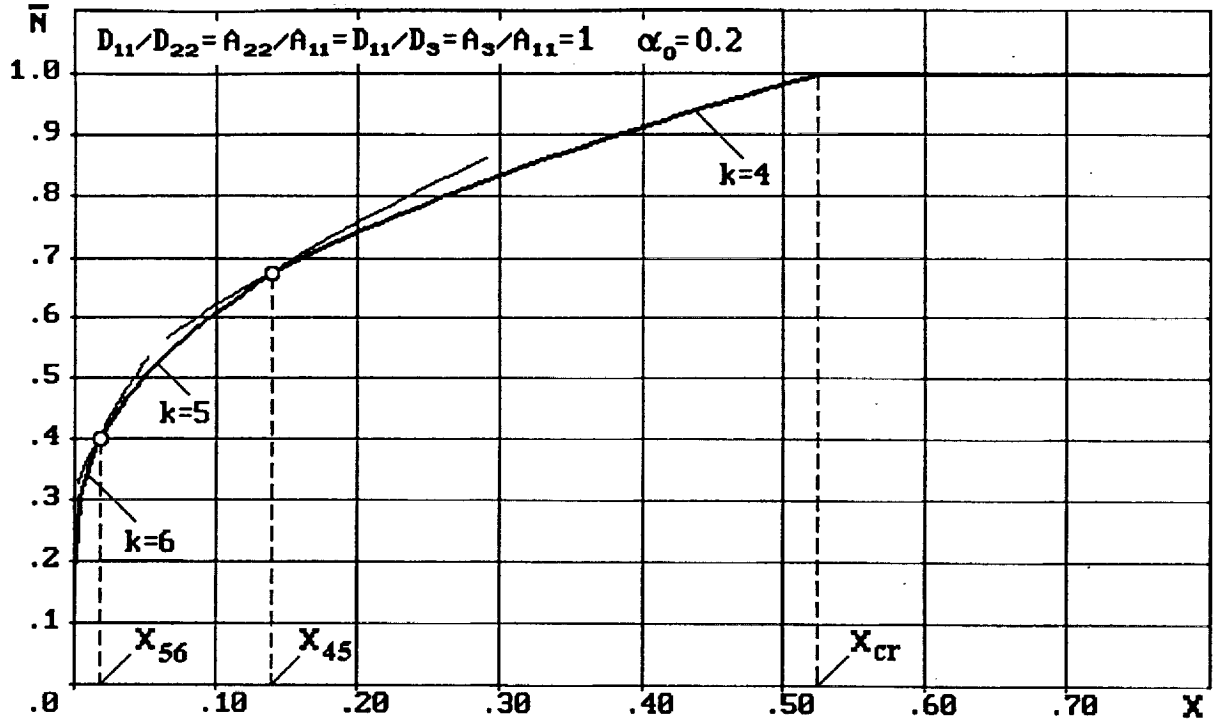


Fig. 1.4

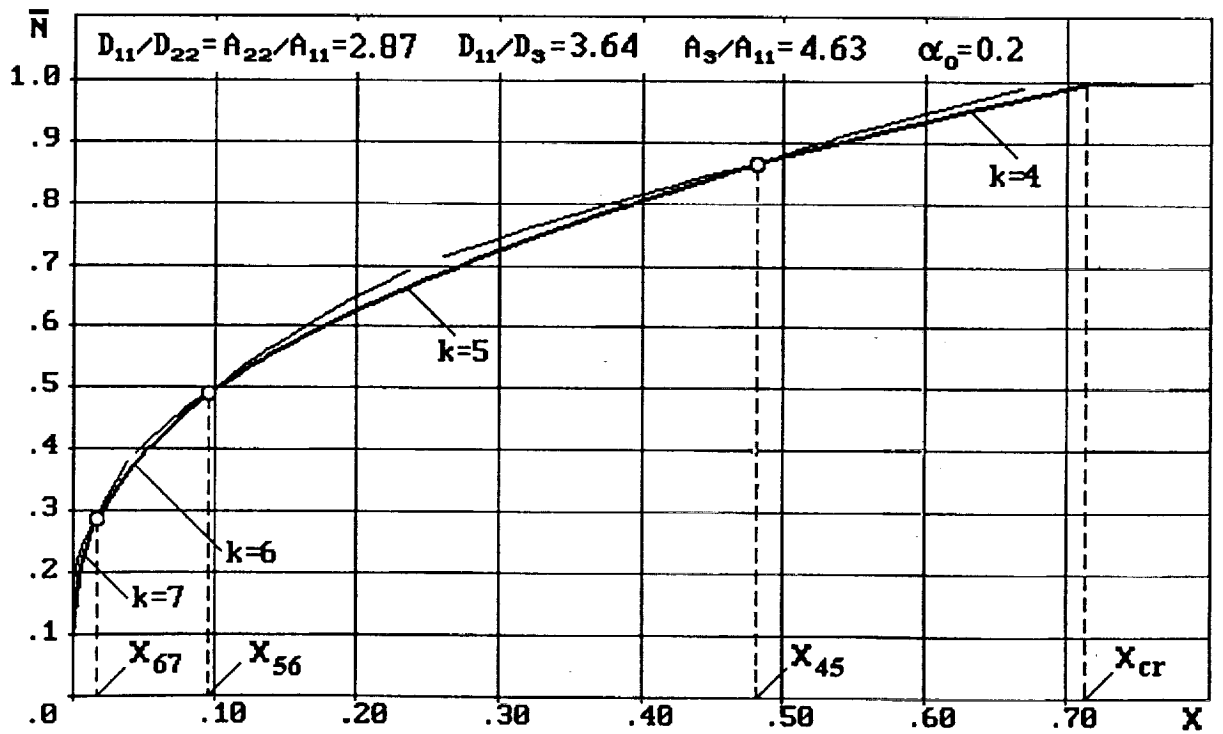


Fig. 1.5

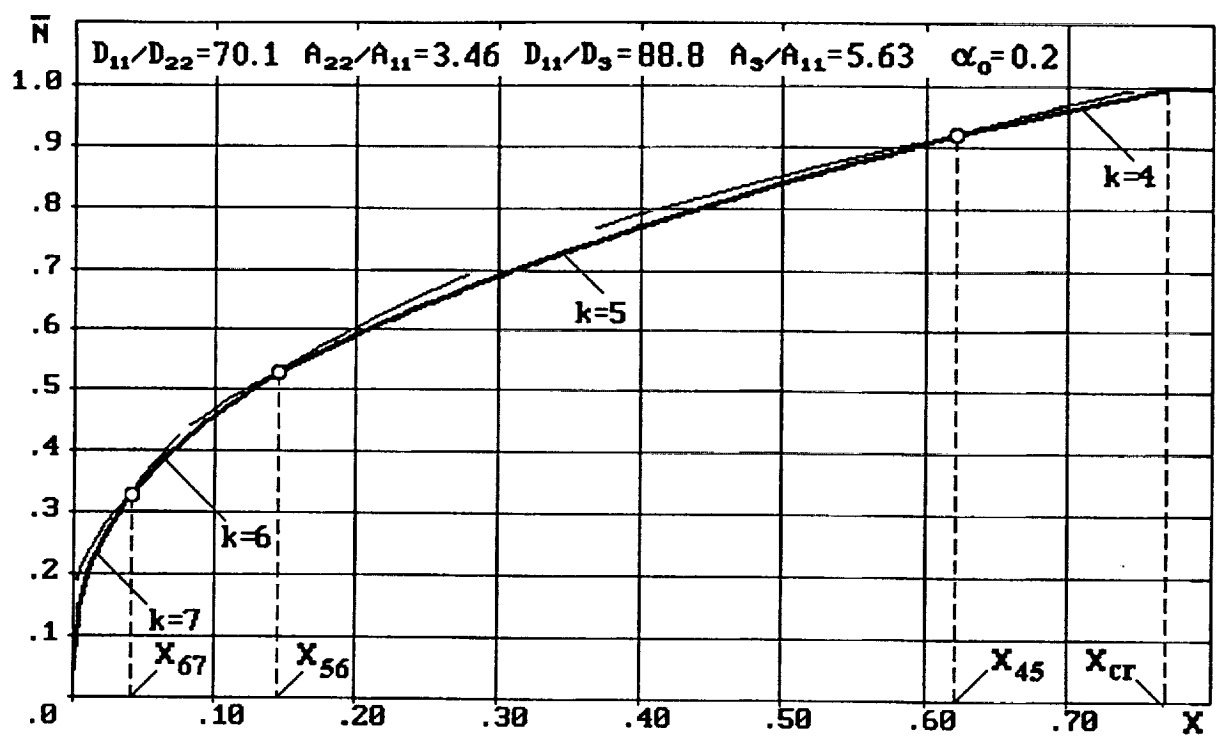


Fig. 1.6

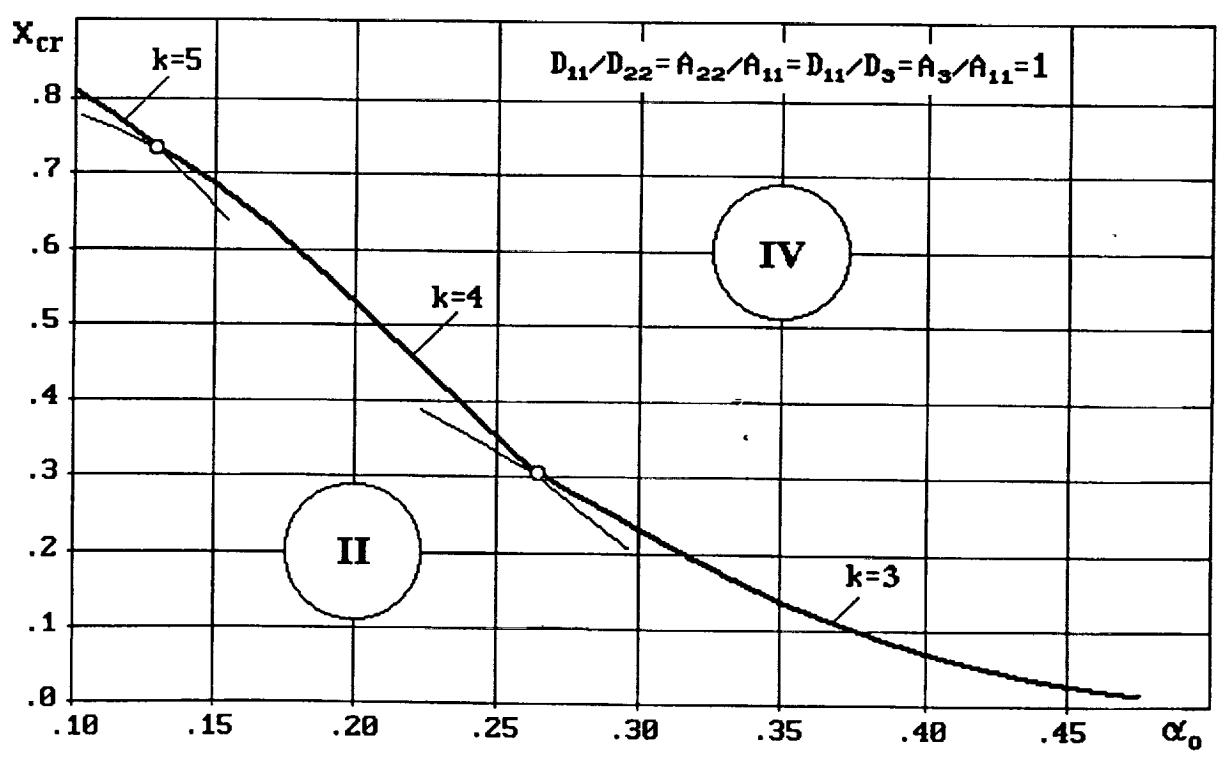


Fig. 1.7

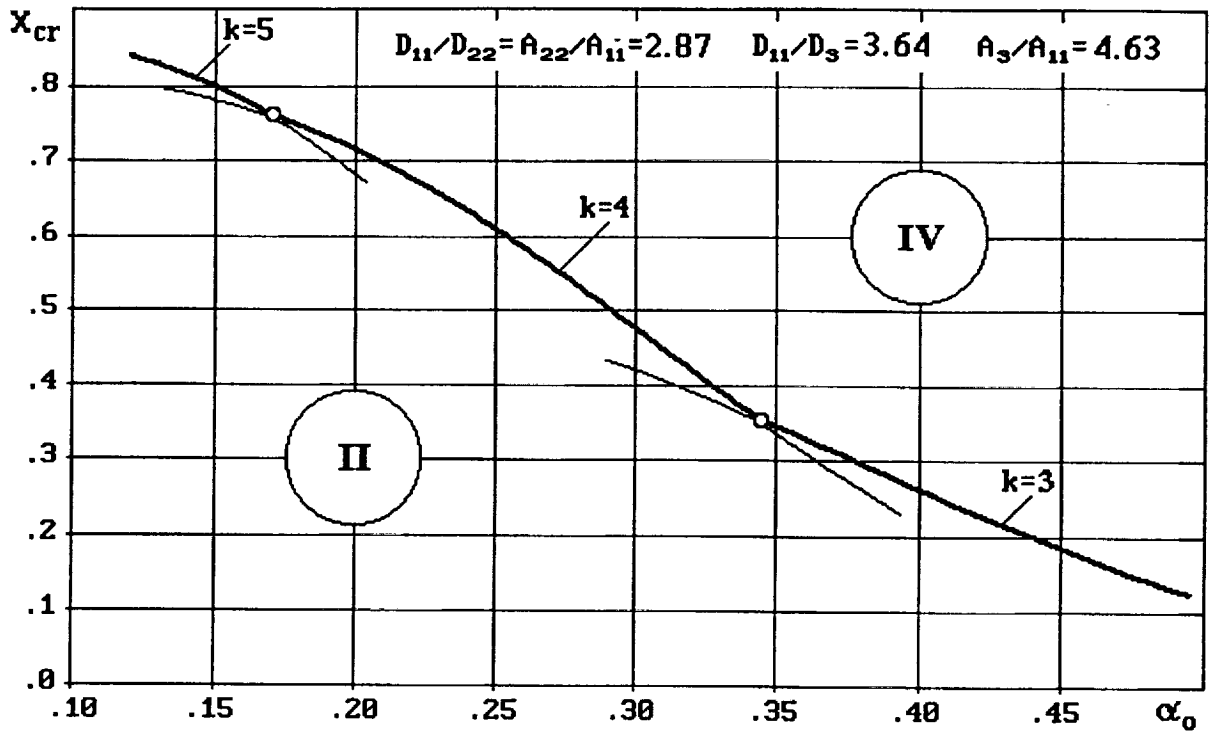


Fig. 1.8

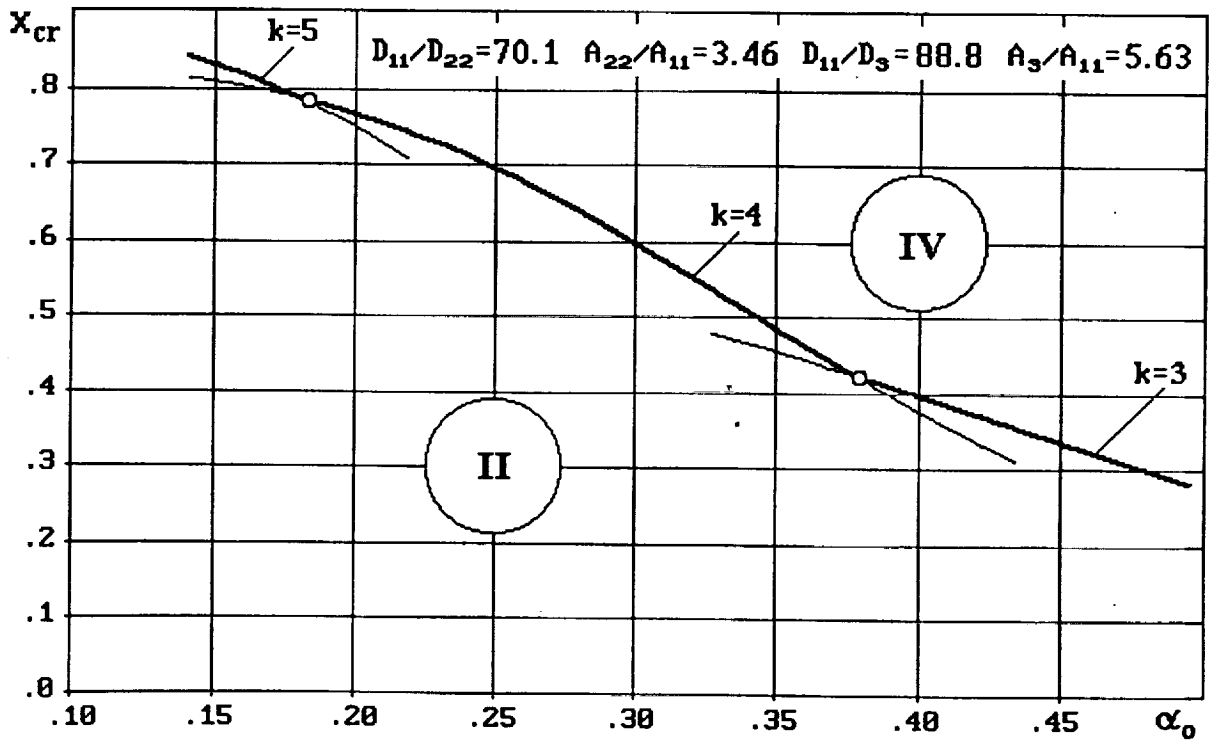


Fig. 1.9

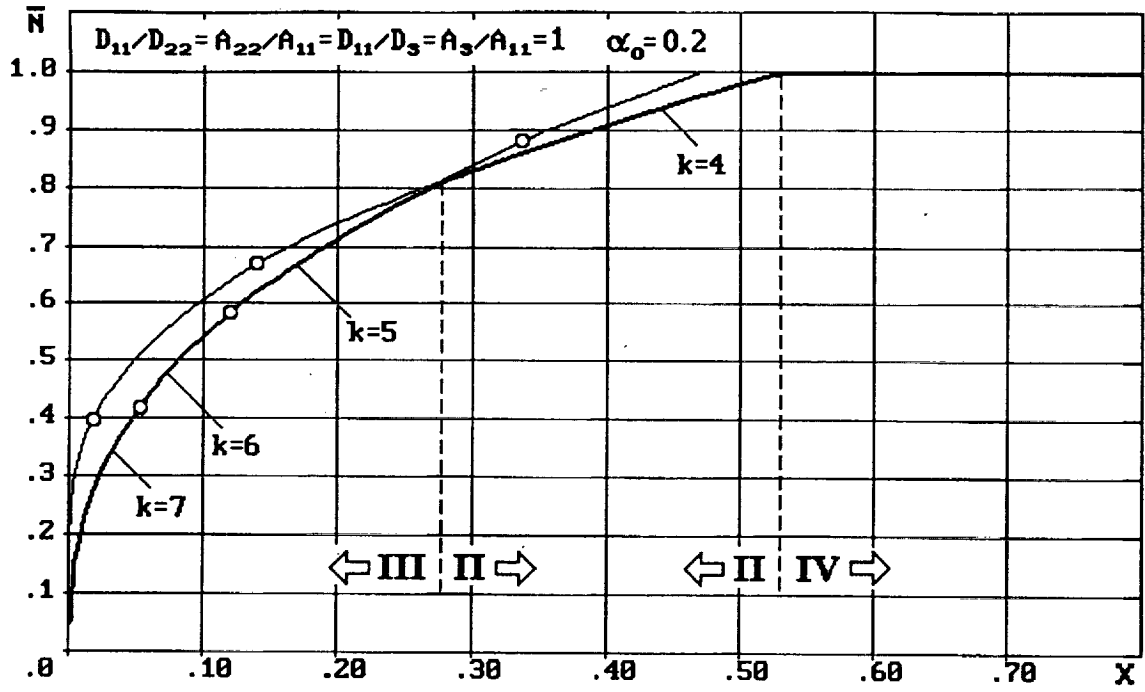


Fig. 1.10

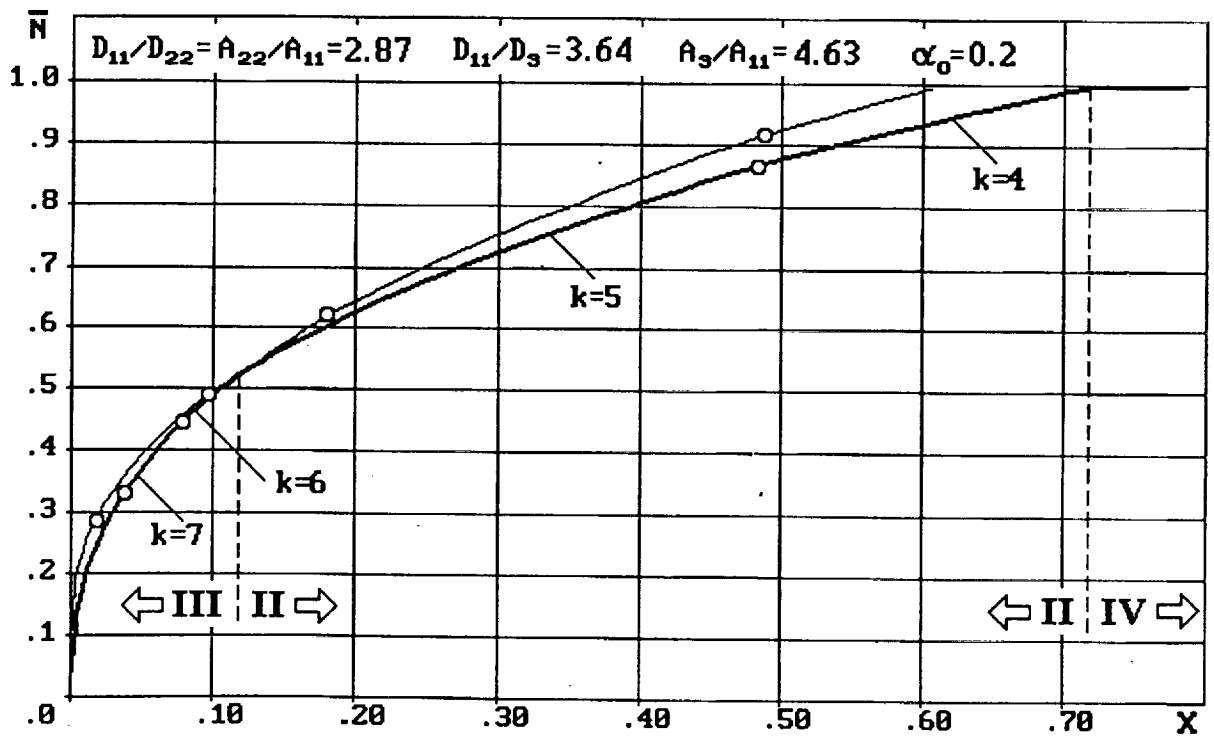


Fig. 1.11

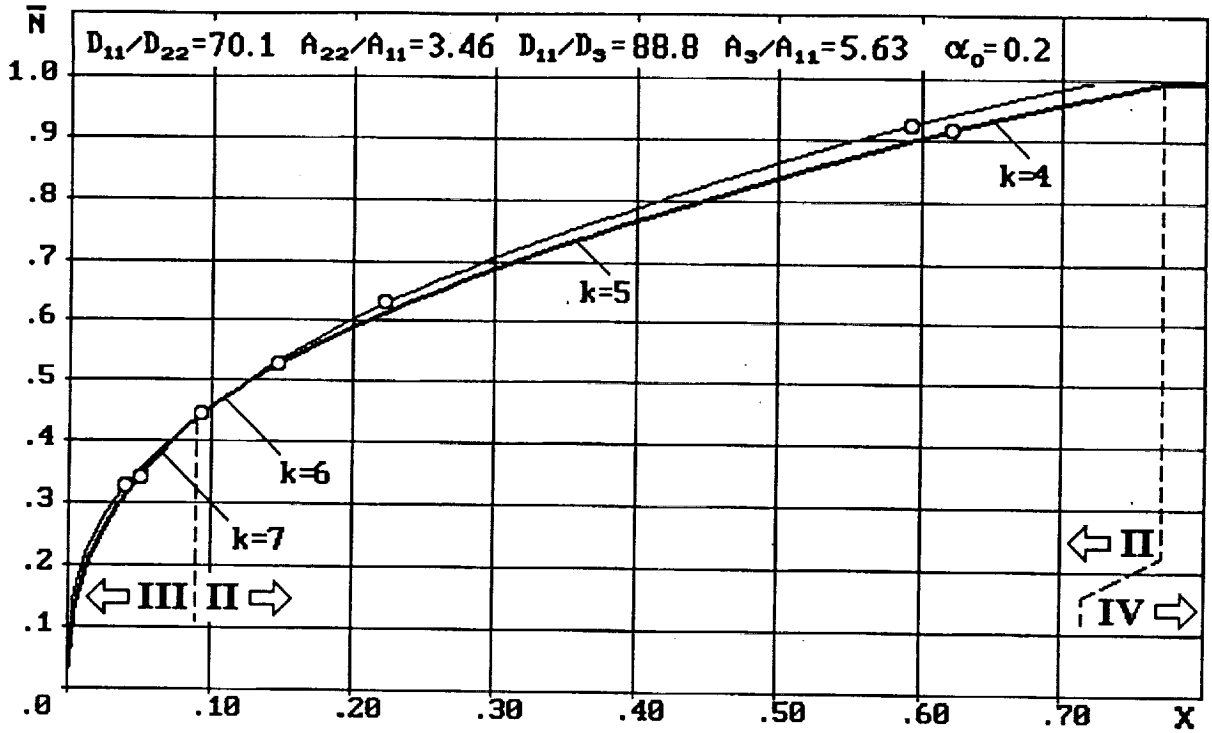


Fig. 1.12

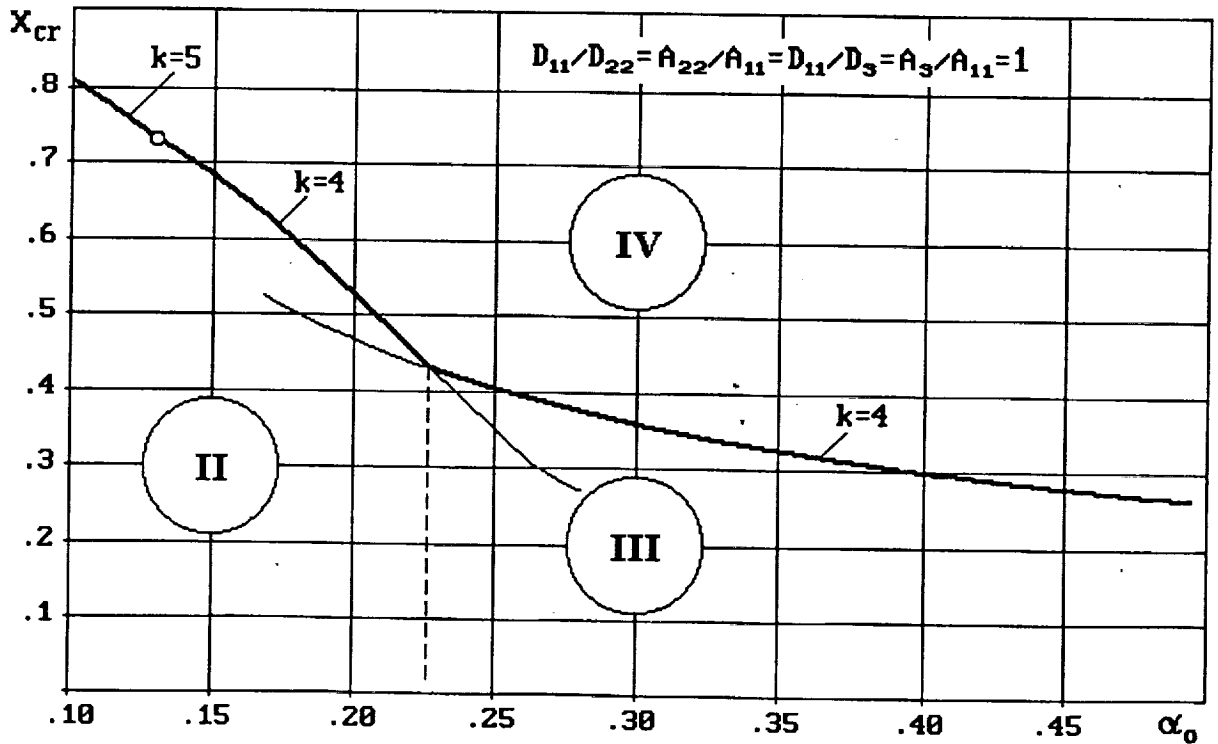


Fig. 1.13

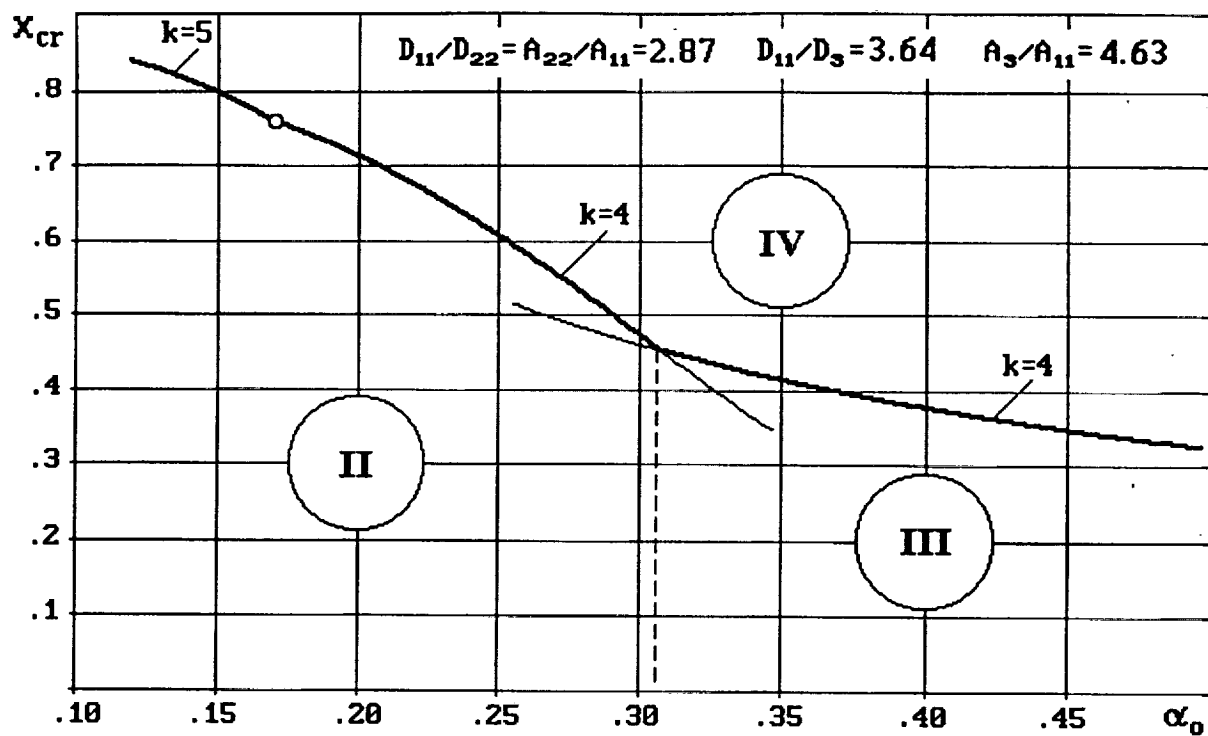


Fig. 1.14

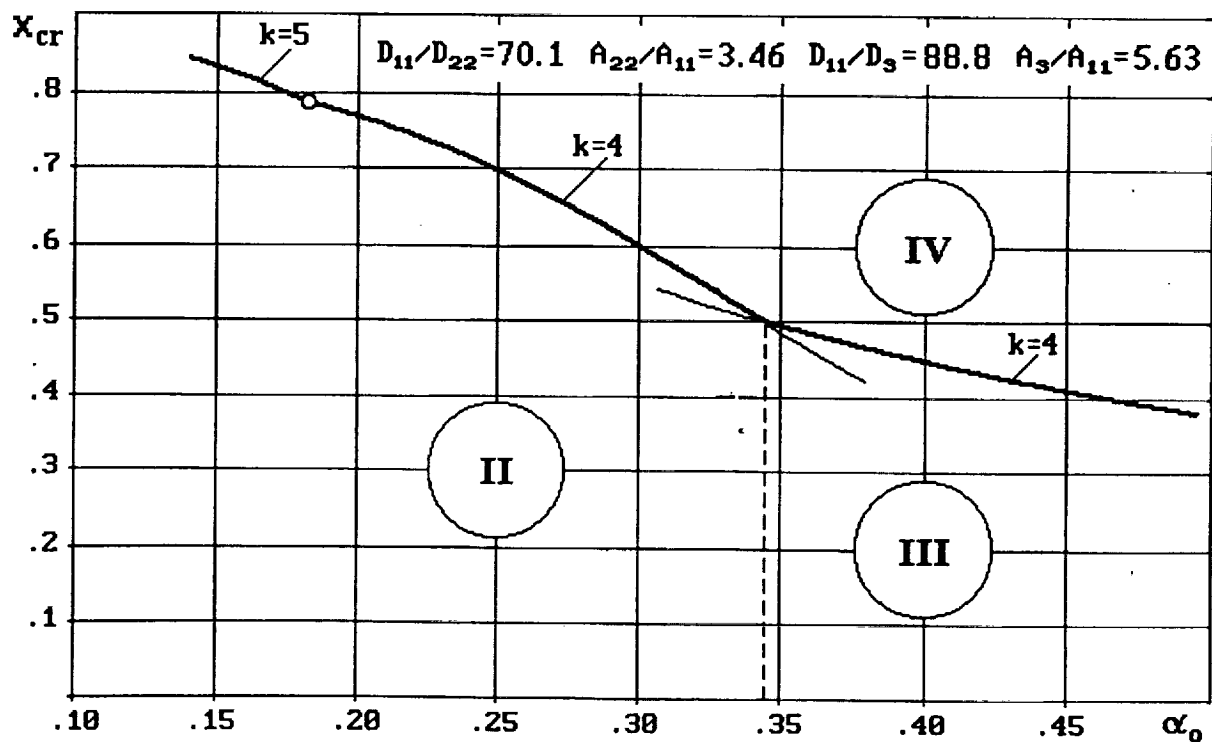


Fig. 1.15

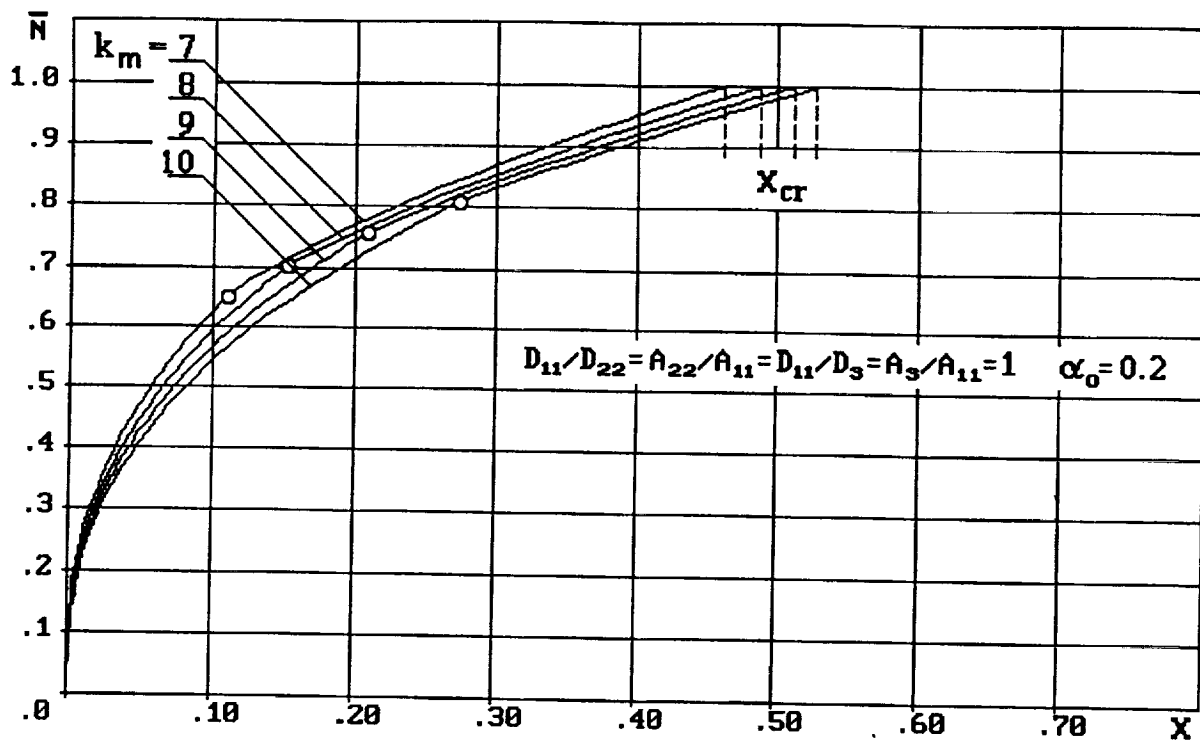


Fig. 1.16

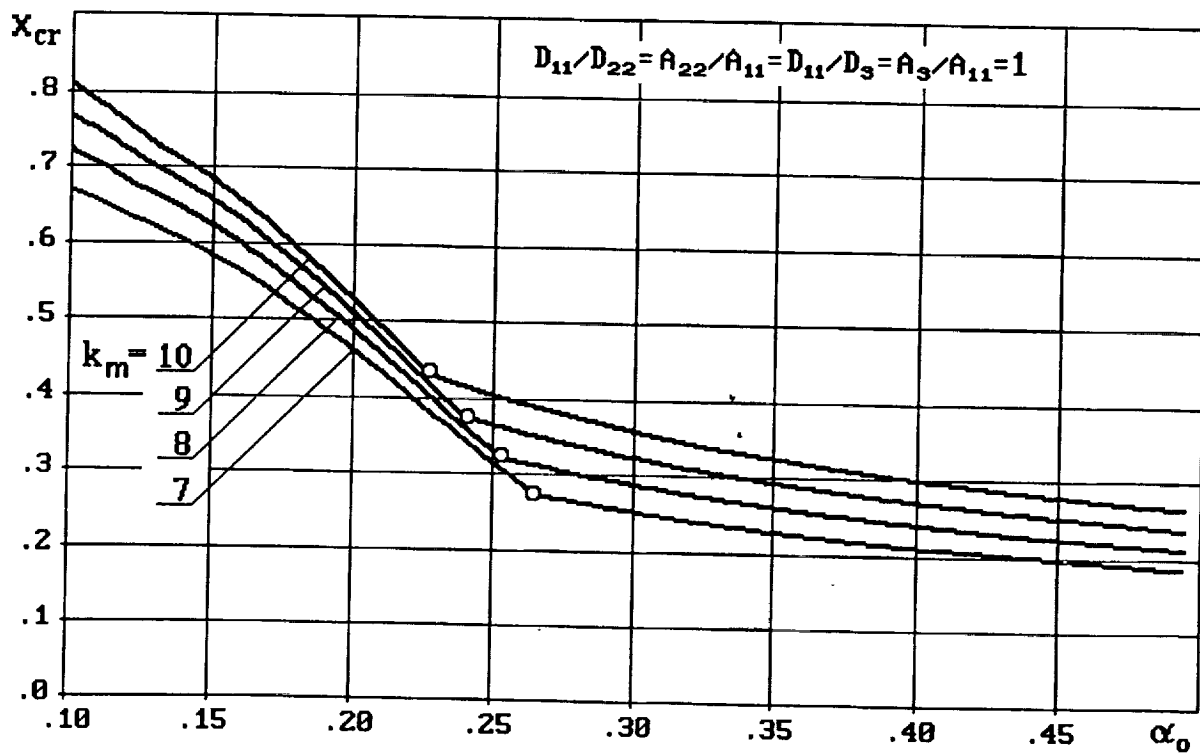


Fig. 1.17

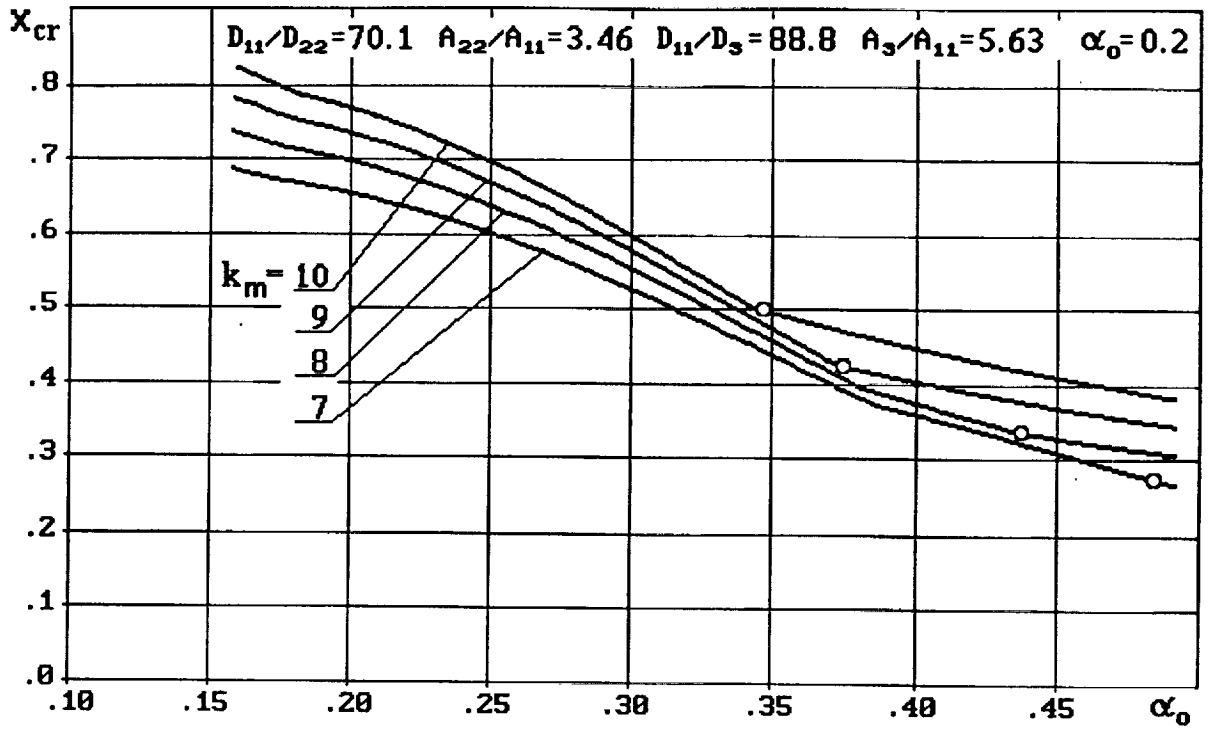


Fig. 1.18

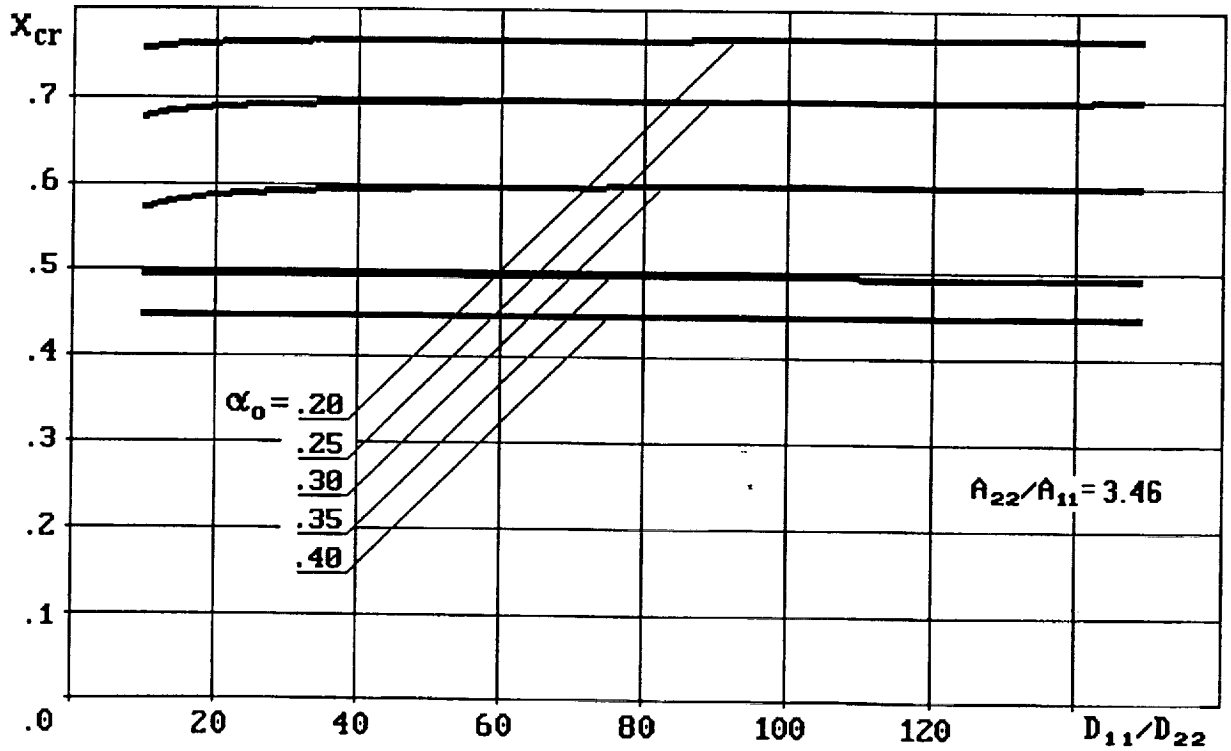


Fig. 1.19

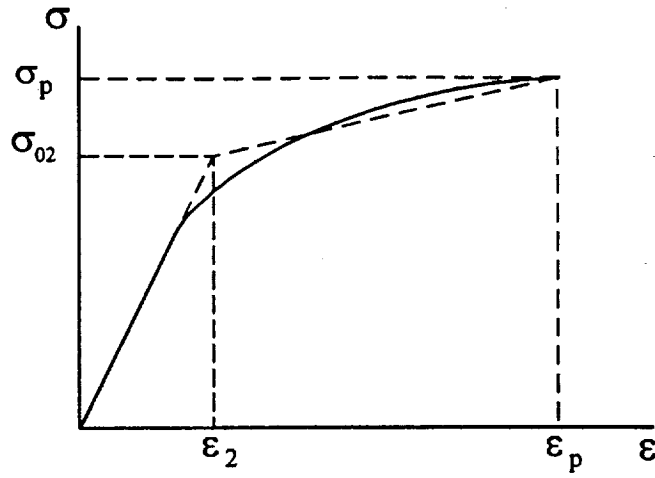


Fig. 2.1

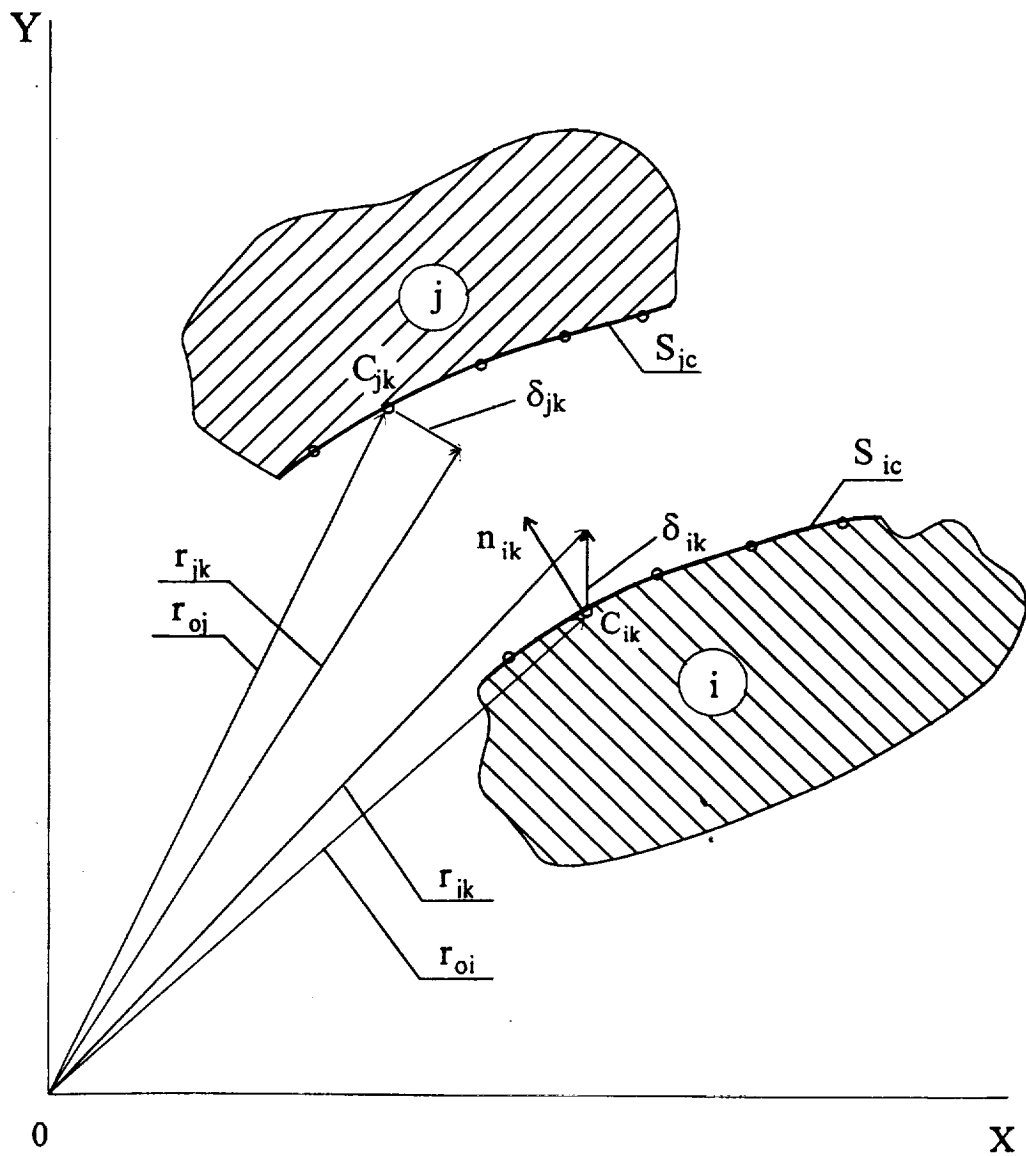


Fig. 2.2

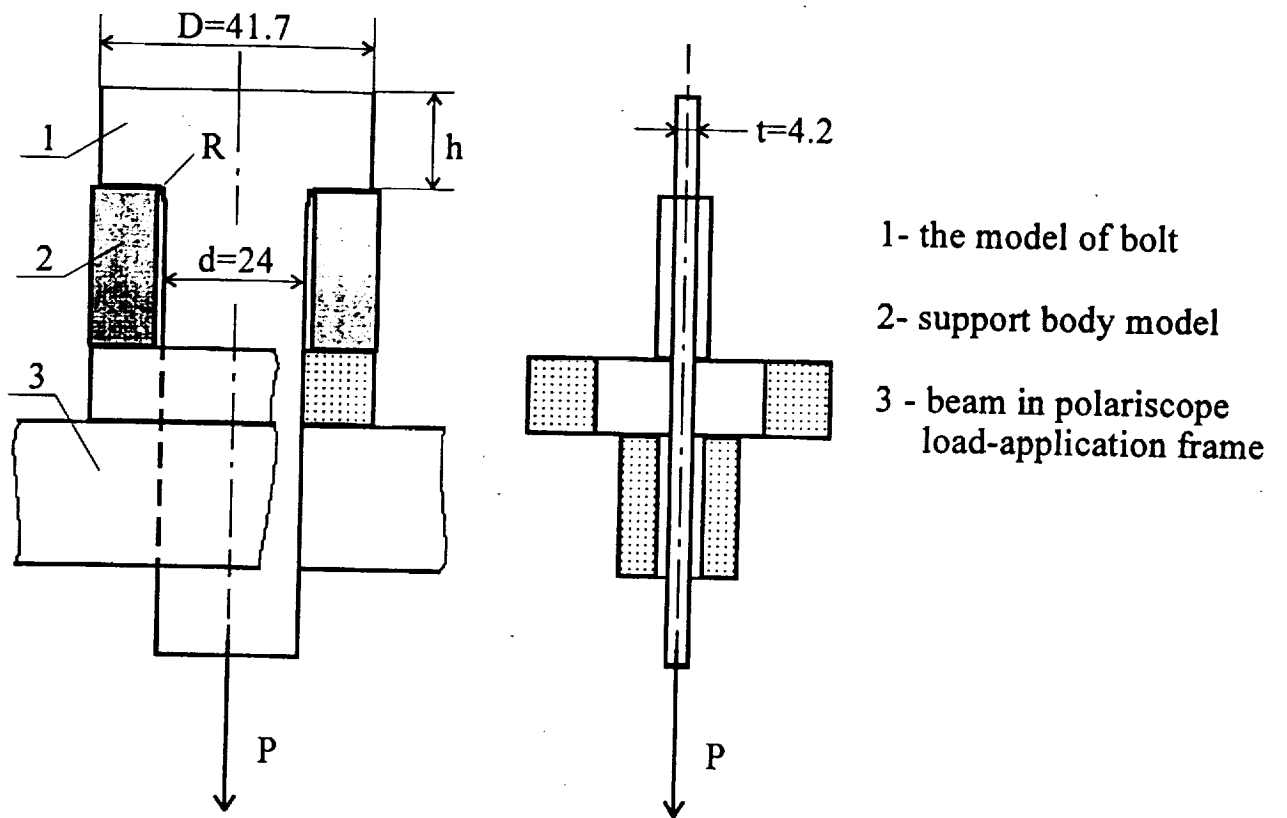


Fig. 2.3

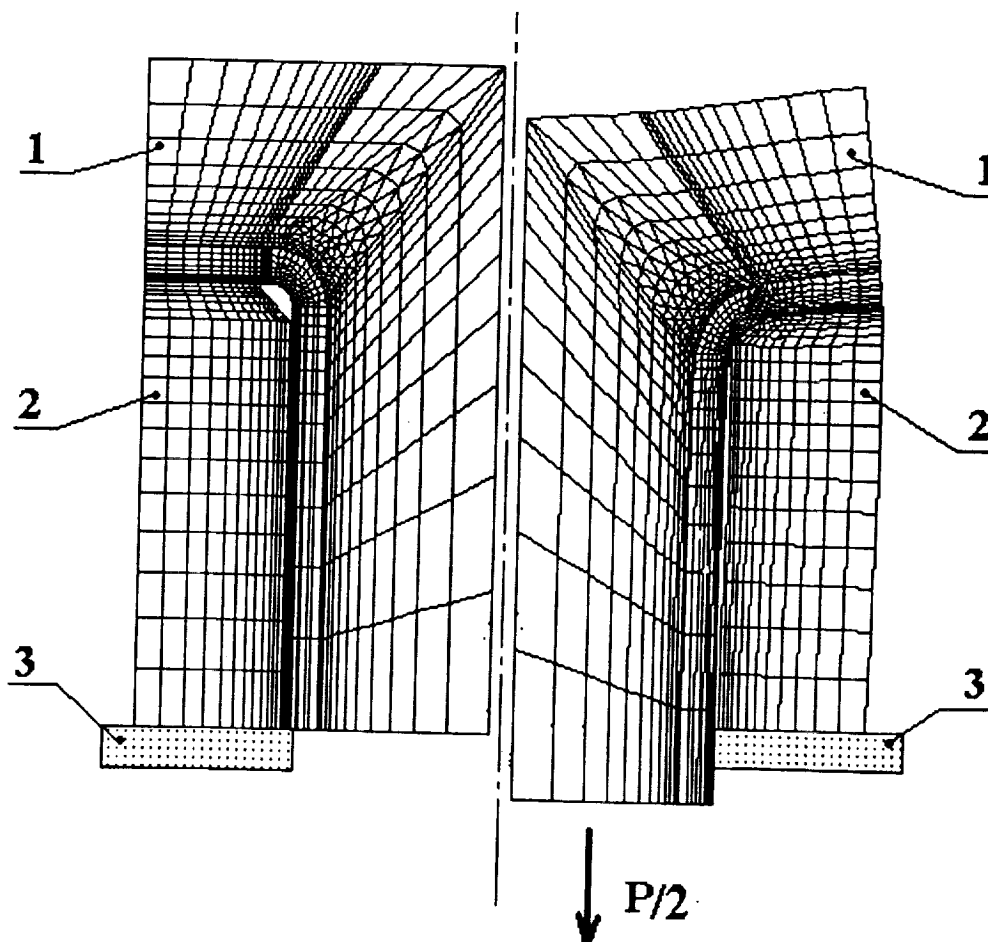


Fig. 2.4

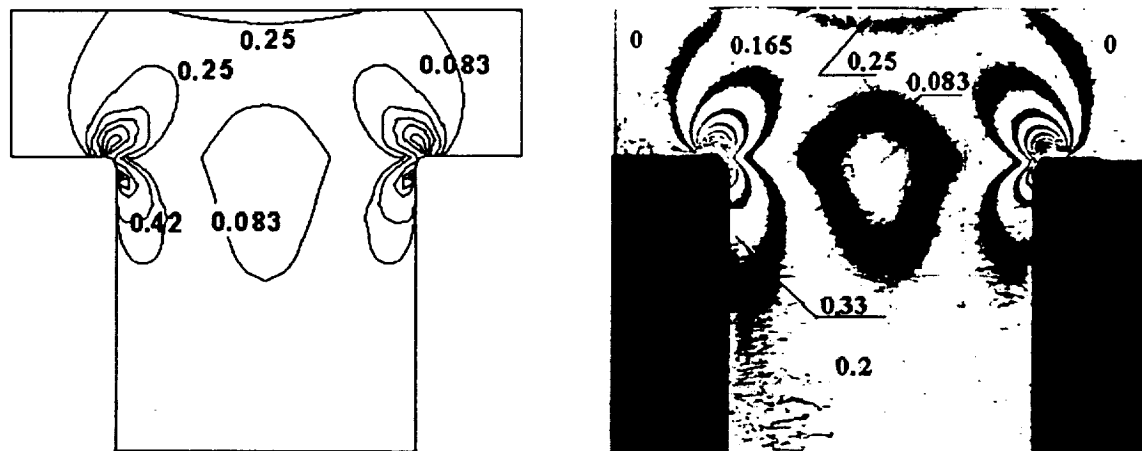


Fig. 2.5

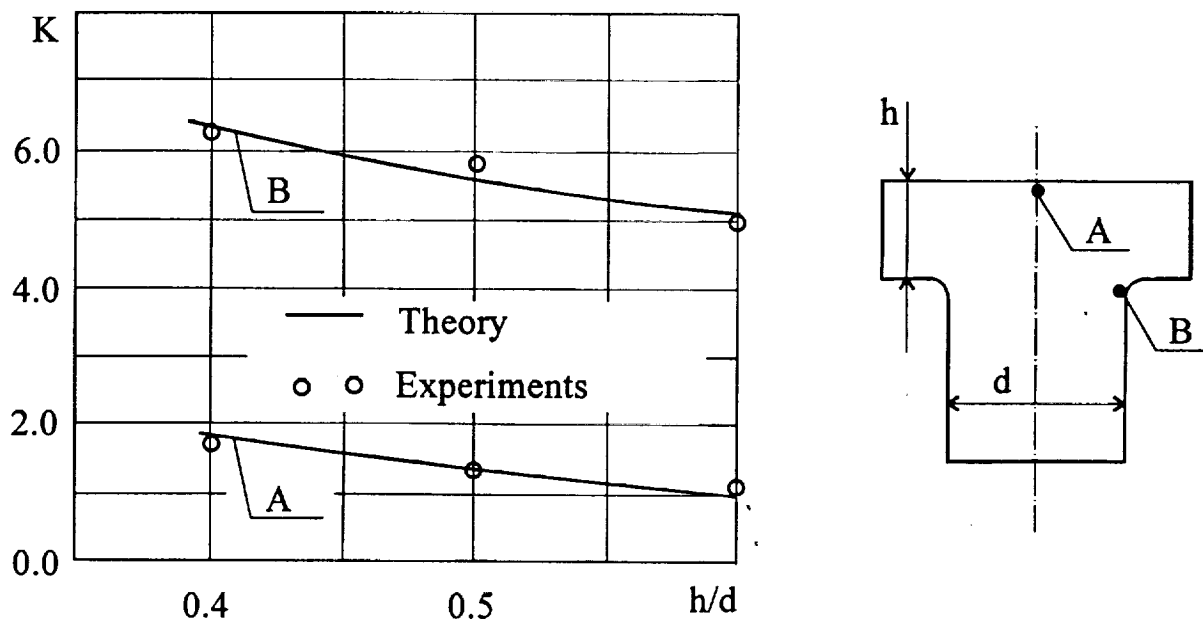
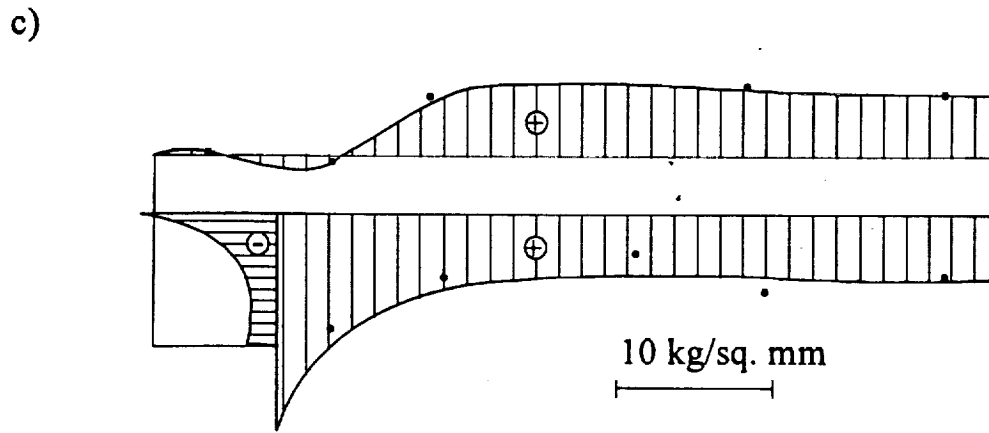
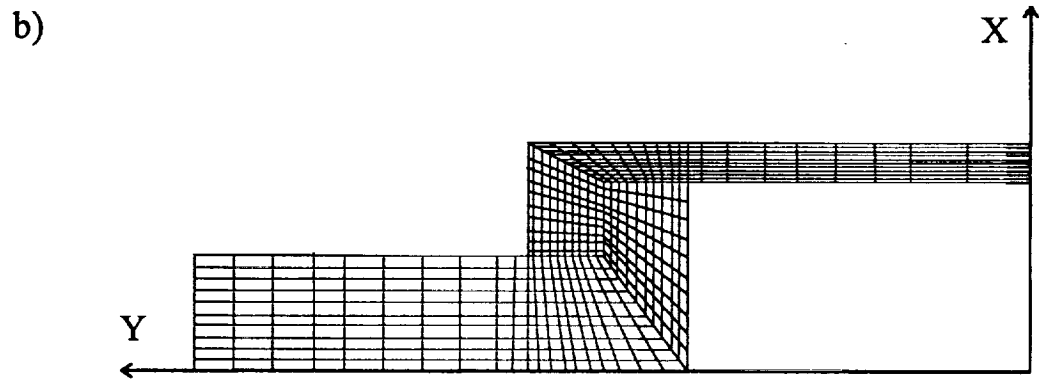
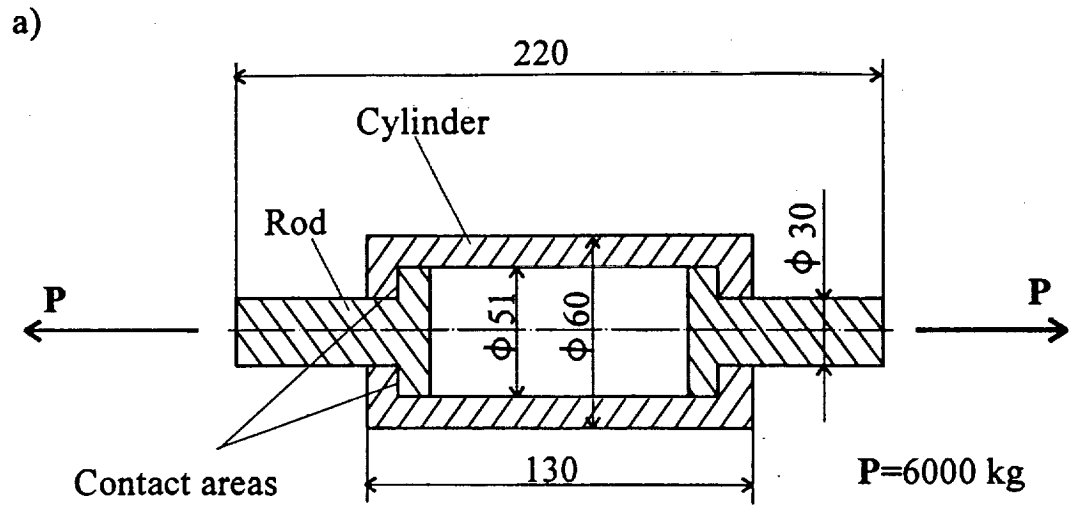


Fig. 2.6



Stress σ_1 in the cylinder:

— finite element method

• experiment

Fig. 2.7

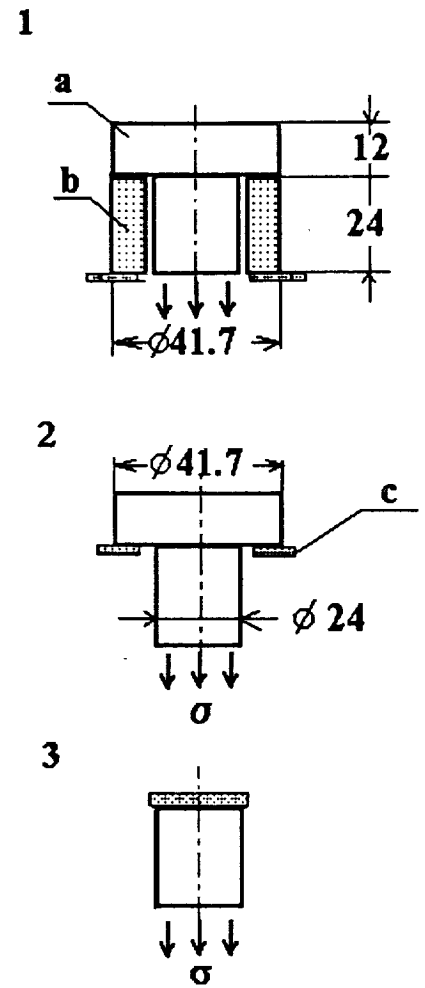
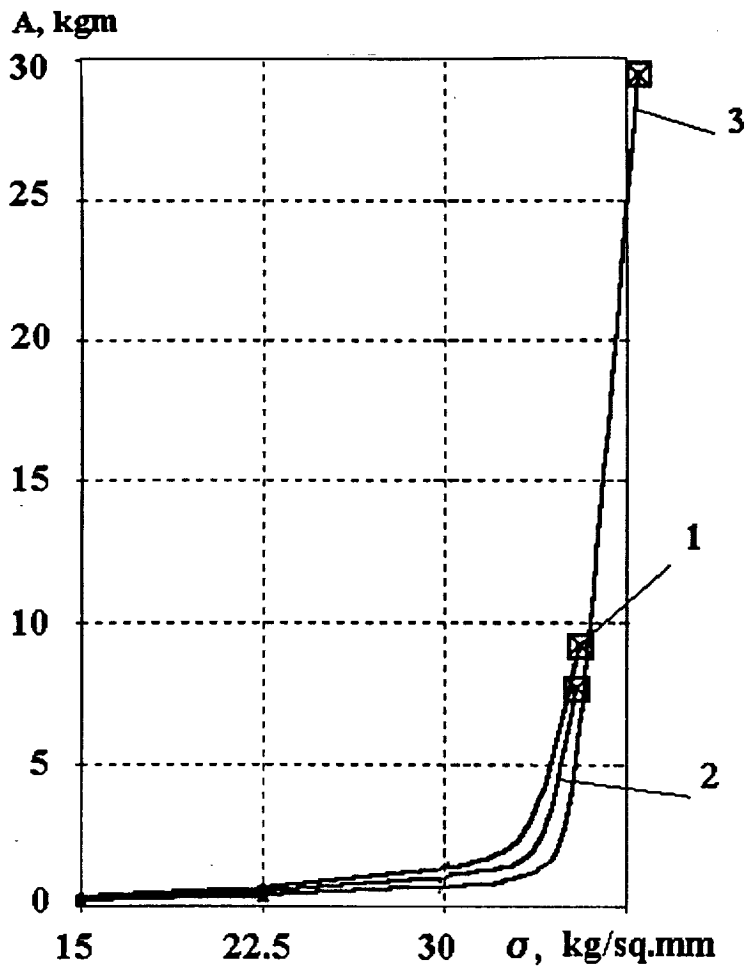


Fig. 2.8

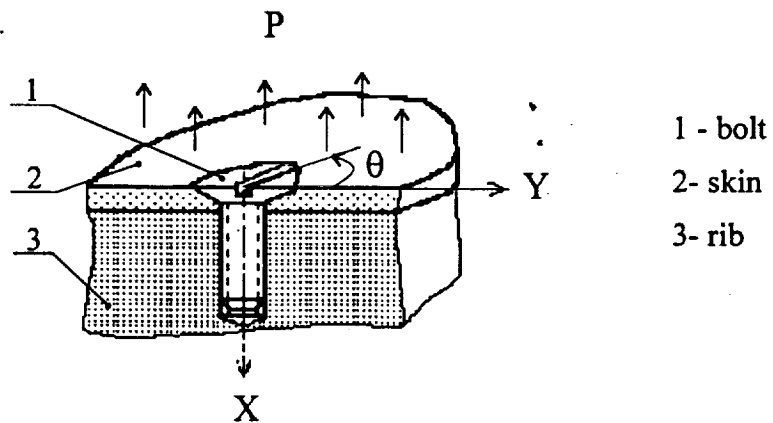


Fig. 2.9

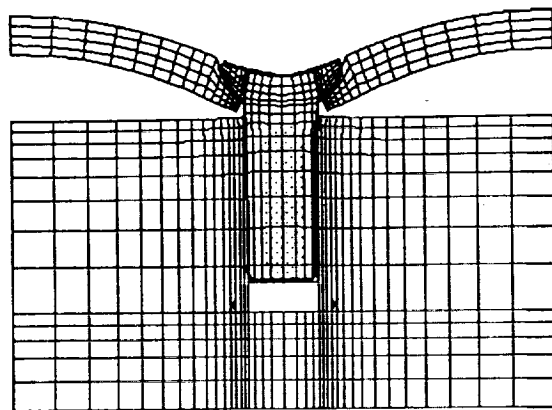


Fig. 2.10

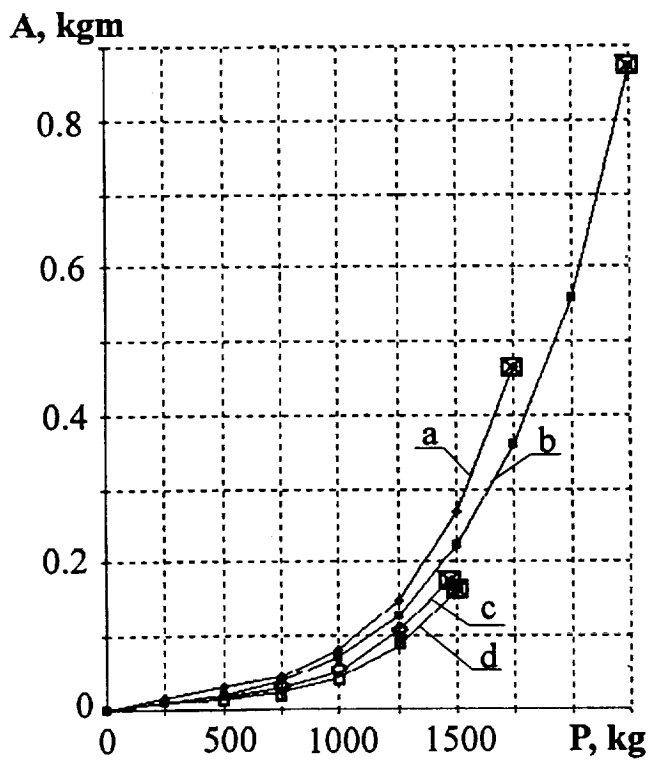
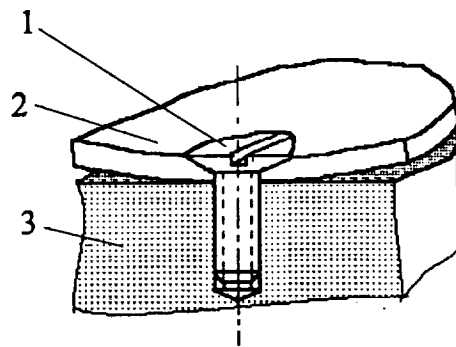


Fig. 2.11



a and c for aluminum bolt
 b and d for steel bolt

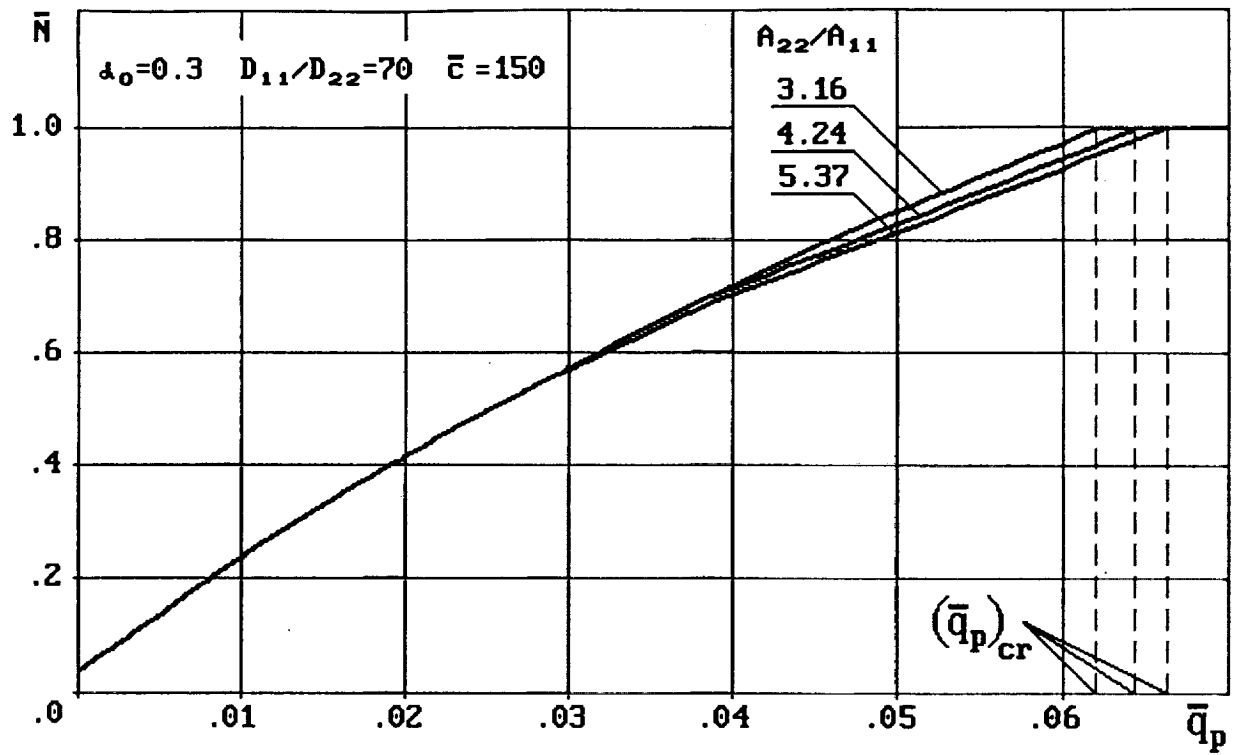


Fig. 2.12

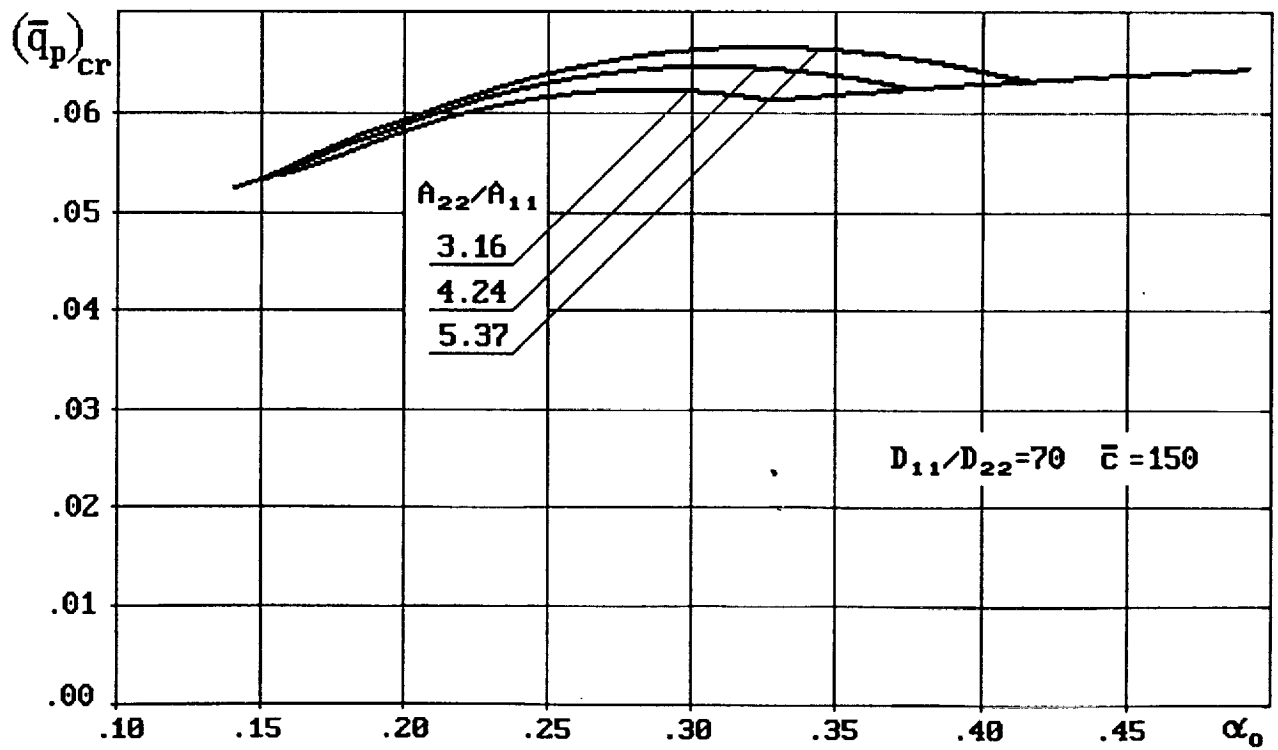


Fig. 2.13

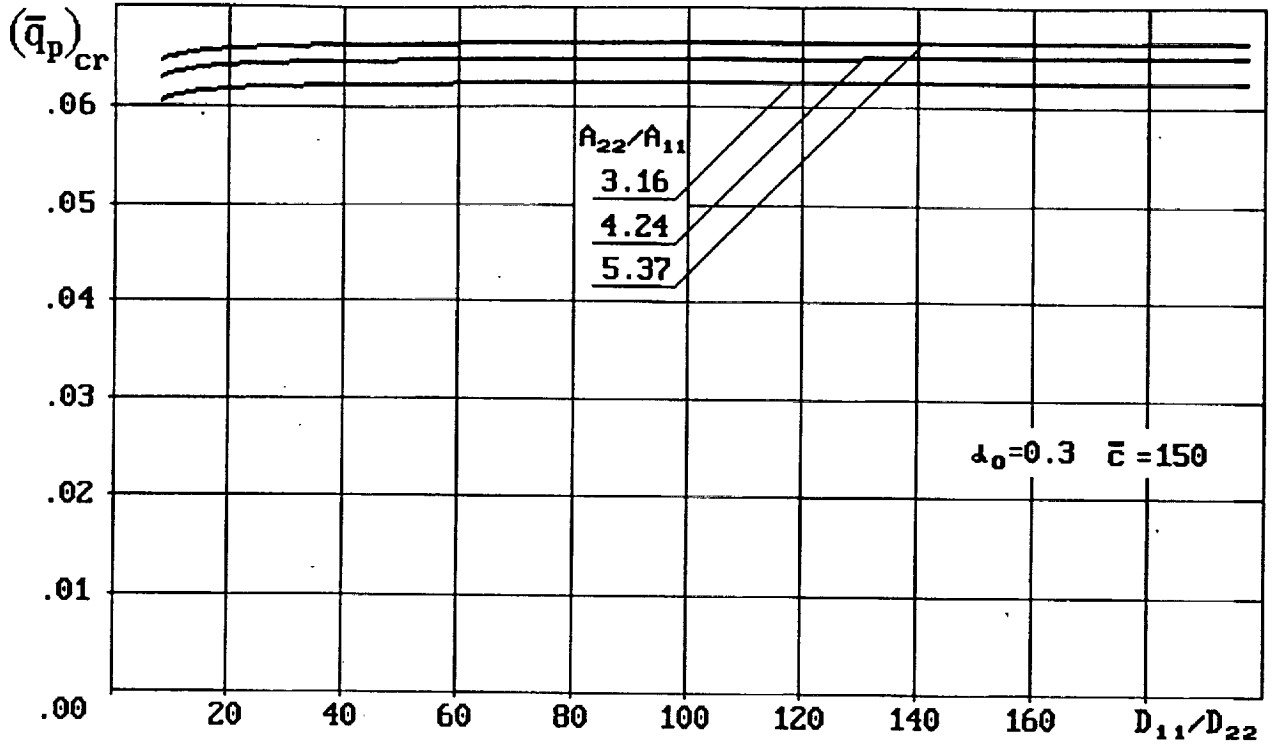


Fig. 2.14

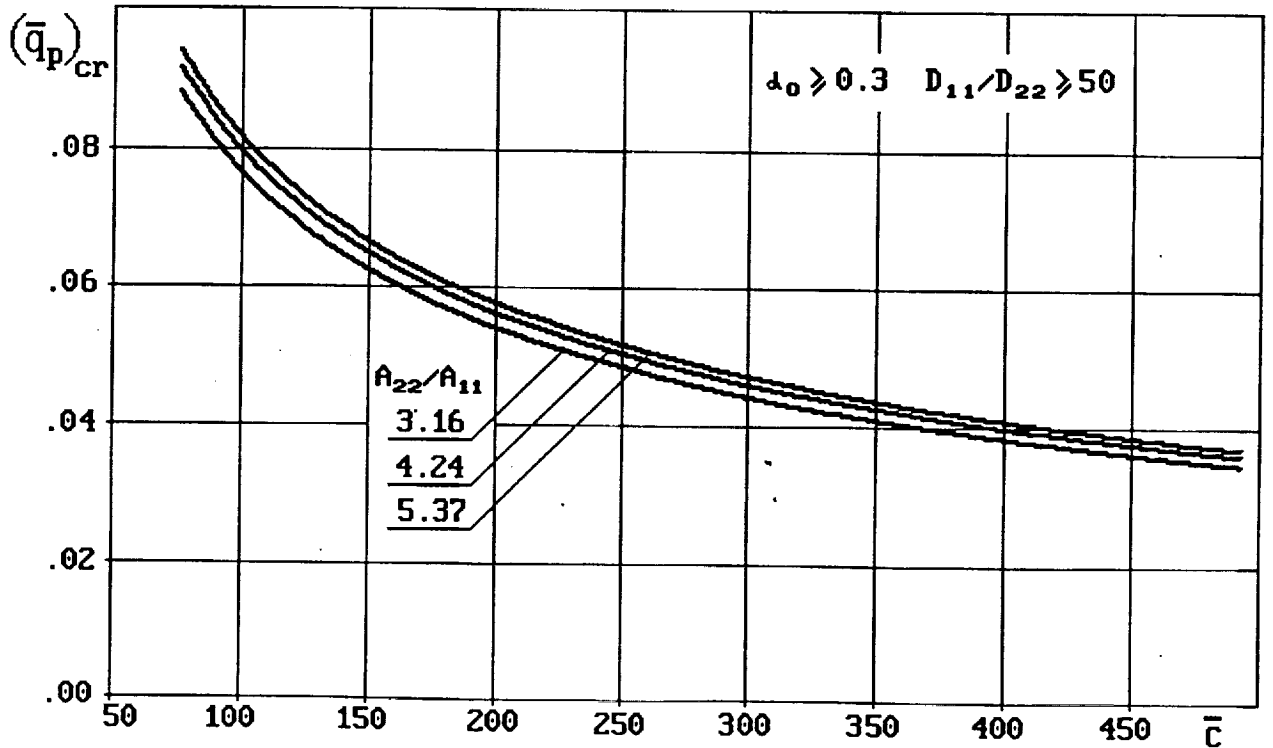


Fig. 2.15